JACK N. AVERITT
COLLEGE
of
GRADUATE
STUDIES
GEORGIA SOUTHERN UNIVERSITY

Georgia Southern University

Digital Commons@Georgia Southern

Fall 2020

A Numerical and Experimental Study on Effect of Composition of Ar-N2 Shielding Gas on the Weld Bead Profile and its Prediction for Hot Wire Arc Additive Manufacturing

Niraj Pudasaini

Follow this and additional works at: https://digitalcommons.georgiasouthern.edu/etd

Part of the Manufacturing Commons, and the Other Mechanical Engineering Commons

A NUMERICAL AND EXPERIMENTAL STUDY ON EFFECT OF COMPOSITION
OF Ar-N$_2$ SHIELDING GAS ON THE WELD BEAD PROFILE AND ITS PREDICTION FOR
HOT WIRE ARC ADDITIVE MANUFACTURING

by

NIRAJ PUDASAINI

(Under the Direction of Bishal Silwal)

ABSTRACT

Wire arc additive manufacturing is a process of making three-dimensional metal parts in a layer-by-layer approach using a feed wire and electric arc as a heat source. Wire arc additive manufacturing (WAAM) is becoming more popular due to its ability to create complex 3D parts, less build time, high deposition rate, and significant cost savings. Out of the many parameters used in WAAM, one of the important parameters is shielding gas which plays a significant role in material quality, properties, and defects. In this study, a controlled amount of argon (Ar) and nitrogen (N$_2$) shielding gases are used to see the effect on the weld bead depth and width. In addition, a computational fluid dynamics (CFD) model is used to perform numerical analysis. The data collected from the experiment is used to perform a regression analysis to predict future values. The amount of shielding gas mixture is controlled through a flowmeter to three different total flowrates. The result shows there is an increase in the depth and width of the weld bead with the increase in N$_2$ percentage in the Ar-N$_2$ shielding gas mixture. With the increase in nitrogen percentage, the tungsten arc is observed unstable and spattering is noticed. The temperature of the surface of the base metal is increased while using the Ar-N$_2$ mixture. The experiment result is further verified by developing and analyzing a three-dimensional computational fluid dynamics model using a volume of fluid (VOF) method. Support vector machine (SVM) regression model with Gaussian kernel function is used to perform the predictive regression analysis. Out of all the regression models, SVM has the lowest model loss for the collected data.

INDEX WORDS: Wire arc additive manufacturing, Shielding gas, CFD, SVM, VOF, Gaussian kernel, Regression analysis, Nitrogen, Argon

A NUMERICAL AND EXPERIMENTAL STUDY ON EFFECT OF COMPOSITION

OF Ar-N$_2$ SHIELDING GAS ON THE WELD BEAD PROFILE AND ITS PREDICTION FOR

HOT WIRE ARC ADDITIVE MANUFACTURING

by

NIRAJ PUDASAINI

B.S., Tribhuvan University, Nepal, 2016

A Thesis Submitted to the Graduate Faculty of Georgia Southern University

in Partial Fulfillment of the Requirements for the Degree

MASTER OF SCIENCE

A NUMERICAL AND EXPERIMENTAL STUDY ON EFFECT OF COMPOSITION
OF AR-N$_2$ SHIELDING GAS ON THE WELD BEAD PROFILE AND ITS PREDICTION FOR
HOT WIRE ARC ADDITIVE MANUFACTURING

by

NIRAJ PUDASAINI

Major Professor: Bishal Silwal

Committee: Marcel Ilie

Hossien Taheri

Electronic Version Approved:

December 2020

DEDICATION

To my mother who never worried about my research, rather worried if I had eaten anything.

ACKNOWLEDGMENTS

TABLE OF CONTENTS

LIST OF TABLES

LIST OF FIGURES

CHAPTER 1: INTRODUCTION

Background

Additive manufacturing is an important research topic due to its approach to industrial production that enables the creation of stronger and lighter parts and systems. There is extensive research going in the field of additive manufacturing because of its benefits in manufacturing than conventional subtractive manufacturing. Additive manufacturing is used in the aerospace industry due to its ability to produce 3D model parts with complex designs, reduce manufacturing costs and fabricate parts with premium materials with small production runs and short turnaround times (Najmon, Raeisi, and Tovar 2019). Additive manufacturing is more popular because of its ability to create stronger and lighter parts and systems and the parts made are more durable than traditionally made parts. Additive manufacturing masters the build time and it is easy to make complex geometries without increasing the cost. Out of the many additive manufacturing techniques, the most popular for creating metal 3D parts are powder bed fusion (PBF) and direct energy deposition.

Wire arc additive manufacturing (WAAM) is a branch of additive manufacturing that uses direct energy deposition technology and uses an arc welding process to make additive 3D metal parts. Unlike the more common metal powder AM processes, WAAM works by melting metal wire using an electric arc (heat source). Wire arc additive manufacturing is becoming more popular because of its ability to create large metal components with a high deposition rate, low equipment cost, high material utilization, and consequent environmental friendliness. The welding wire is significantly less expensive than metal powder used in metal powder bed fusion hence greatly reducing the material costs. Compared to other techniques WAAM parts have a major problem of residual stress and poor surface finish. In wire arc additive manufacturing, one of the main

components that affect the printed parts is shielding gas. As air, hydrocarbons, and moisture lead the printed parts to distortion, shielding gases are used to protect the part from any reaction from the ambient atmosphere. Different shielding gases have different properties hence it greatly affects the weld pool morphology. One of the most used primary shielding gas in tungsten arc welding is argon. Besides argon the secondary shielding gases used are carbon dioxide, helium, nitrogen, etc. The addition of these secondary shielding gases to primary argon shielding gas has shown the change in heat flux and arc temperature ultimately affecting the welding pool height and width.

Problem Statement

In wire arc additive manufacturing, one of the main components that affect the printed parts is shielding gas. As air, hydrocarbons, and moisture lead the printed parts to distortion, shielding gases are used to protect the part from any reaction from the ambient atmosphere. The physical and chemical properties of shielding gases used also affect the arc and weld properties as metal transfer, oxidation, porosity, slag formation, penetration, fusion, and spatter (Lucas 1992). Also, it is experimentally verified that the shielding gases can be used as a surface-active element to improve the depth/width ratio of the weld (Heiple et al. 1983). Surface oxides are one of the main problems on WAAM structure which destabilize the arc and weld pool causing harm to surface finish. An extra tent shielding is found to improve the surface waviness and deposition efficiency in that case (Xu et al. 2018).

Mostly inert gases are used as shielding gas because of their inactivity in a chemical reaction. But a certain amount of addition of any other gases can make the weld better or worse in some cases. The addition of hydrogen to argon gives an arc a wider temperature distribution and a larger heat input (Heiple et al. 1983). An increment of hydrogen content in shielding gas contributes to an increase in penetration depth and the cross-section area of the weld metal both

with and without an activating flux (Huang 2010). Similarly, a study of the addition of nitrogen to the argon shielding gas was done which shows the magnitude of heat input is increased after the addition of nitrogen (K. Tseng and Chou 2002). Another similar study of the effect of shielding gas composition shows the increment of nitrogen in argon-based shielding gas in the range of 2.5-10 vol% shows the increment in the penetration and cross-sectional area of the weld (Huang 2009). An increment in carbon dioxide leads to a decrease in the amount of porosity but the weld metal hardness decreases (Ebrahimnia et al. 2009). The addition of shielding gas does not always mean the bead will get stronger and better. A study of the effect of the addition of nitrogen in argon shielding gas on weld bead morphology of the P91 ferritic/martensitic steel shows unstable arc, spattering, and porosities formation (Vidyarthy and Dwivedi 2019). All these studies show the increase in the width and depth after addition of some secondary shielding gases like nitrogen, carbon dioxide, and hydrogen. So, a parametric study is necessary to see the rate of change of weld bead dimensions with the tiny increment in the secondary shielding gas (nitrogen).

Machine learning is a growing field that helps to predict the output based on the algorithm created on the previous data. These days machine learning is being popular in the welding area so that the algorithm created can help to predict the future weld bead parameters like penetration depth, height, and bead structure. Similarly, the defects in the weld can be predicted by using machine learning tools like Decision Trees, Artificial Neural Network (ANN), Fuzzy logic, Support Vector Machines (SVM), and others. The algorithm using Support Vector Regression (SVR) to predict the weld joint penetration shows the SVR method performs better for the small amount of data than the multilayer perceptron artificial neural network model (Liang et al. 2019). A study using arc sound to predict the weld quality monitoring shows the efficiency of 88.69% using random forest and 70.78% using the J48 algorithm (Sumesh et al. 2015). ANN and SVR are

the main two algorithms used in the prediction of future weld parameters and morphology. It is seen that with the small amount of data SVR is effective while in the case of a large amount of data ANN is more effective. The prediction of bead geometry using a two-stage SVM-ANN algorithm for TIG welds can avoid overestimation of the mechanical properties and can have both features of SVM and ANN (Kshirsagar et al. 2019). The prediction analysis algorithm of weld depth and width with the use of two different shielding gases helps to predict the future results and see the effect more clearly. Also, the prediction analysis helps to see the trend in the experimental results and how it deviates in a manner that has not been seen before.

Objectives

The main objective of this study is to analyze the effect of the use of different shielding gases, one pure argon and another mixture of argon and nitrogen in weld bead to see which gives more refined geometry of the additively manufactured material. Specific objectives include:

1. Develop and verify the computational fluid dynamics model using a volume of fluid (method) to understand the effect of the above-mentioned gas mixture.

    a. Mass equation, continuity equation, energy equation

    b. Boundary conditions – heat flux, heat loss due to conduction, radiation, convection, evaporation

    c. Arc pressure, electromagnetic force

    d. Droplet impact – higher than the effect of c.

    e. Calculation of heat flux for the simulation.

2. Analyze the effect of adding nitrogen in argon shielding gas on the weld-bead geometry

    a. Variables - Flow rate

    b. Variables - Percentage composition

3. Develop a machine learning algorithm to predict the weld-bead dimensions (width and height)

Significance

The addition of secondary shielding gas to the primary gas affects the weld pool depth and width. The understanding of this change of this depth and width in the weld pool of the weld metal helps to fabricate the 3D metal parts of the desired choice in additive manufacturing. A greater height of the 3D metal parts is desired if the finishing time is important while a greater depth of the 3D metal parts is desired if the strength is important. So, understanding the change in depth and width of the weld pool ultimately benefits the choice of fabrication of 3D metal parts. Also, the machine learning algorithm developed in the study helps to predict the future weld depth and width and perform the prediction analysis. The prediction analysis helps to figure out the trend of experimental data and notice the outliers.

CHAPTER 2: LITERATURE REVIEW

Computational Fluid Dynamics

Computational fluid dynamics (CFD) uses numerical calculations to simulate the flow of the fluid, and the interaction of the fluid with surfaces defined by specific boundary conditions. It is widely used in the fields of aerodynamics, aerospace, weather prediction, industrial system design, biological engineering, fluid flows and heat transfer, and combustion analysis. The basic equation used for the calculation of most of the CFD problems is the Navier-Stokes equation (Harlow and Welch 1965). In computational fluid dynamics, the volume of fluid (VOF) method is a numerical technique for tracking and locating the fluid-fluid interface. It is based on the volume-of-fluid function which gives the fractional volume of one of the fluids in each mesh of the finite difference grid (Renardy, Renardy, and Li 2001). Transient analysis of the welding simulation can detect free surface variation during the simulation time. VOF method is a type of transient analysis method that can track the molten pool surface (D.W. Cho et al. 2013). Previous studies show that the weld pool convection is driven by a combination of forces, namely the surface tension force, buoyancy force, electromagnetic force, and drag force (Fan, Tsai, and Na 2001).

The addition of filler metal is always the most important challenge in the CFD of TIG welding. The simulation of the GTAW process can be done by artificially adding the molten droplets in a computational domain from a specific height above the base plate (J. Cho and Na 2009). Computational methods are also used to calculate the gas tungsten arc welding properties in a unified system of electrodes, arc, and workpiece. Previous study on the CFD of the electrode arc in TIG welding shows that the addition of hydrogen gas in argon makes the arc more constricted, increase the arc temperature and voltage, and increase the volume of the molten

material of the workpiece for a given arc current (Lowke et al. 1997). The falling molten drops carry mass, momentum, and thermal energy, and periodically impinge into the weld pool. The heat transfer and fluid flow are calculated in computational fluid dynamics by the numerical solution of governing equations in a three-dimensional space (Cao, Yang, and Chen 2004). The governing equations are the mass continuity equation, momentum equation, and energy equation. The computational method and governing equations are briefly discussed in the methodology section.

Heat distribution

The source of heat in melting the base metal and filler rod in TIG welding is the tungsten arc. Therefore, an electric arc should be accurately modeled to get the correct temperature distributions in the model results. The heat source model is considered as the most important boundary condition in the numerical thermal analysis. The previous study on the heat model shows the use of different heat distribution models. A volumetric heat source model is the double ellipsoid distribution with spherical and cylindrical volumes along the thickness of the model (C. Wu, Hu, and Gao 2009). The volumetric double ellipsoid heat source model also known as Goldak's model is built of two ellipsoids perpendicular to each other (Kik 2020).
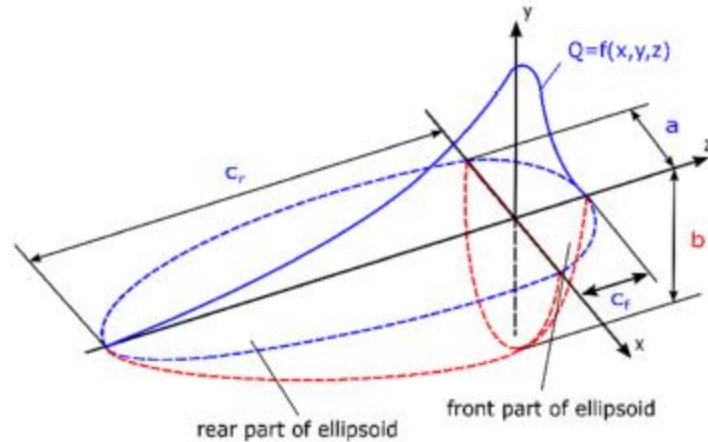
Figure 1. Double ellipsoid heat source model (Kik and Górka 2019).

Unlike other models used for arc welding simulations, a double ellipsoid model is described by two equations for each part of an ellipsoid (Kik and Górka 2019). The equation for the front part of an ellipsoid is:

$$Q_f(x, y, z) = \frac{6\sqrt{3}f_f Q}{abC_f\pi\sqrt{\pi}} exp\left(\frac{-kx^2}{a^2}\right) exp\left(\frac{-ly^2}{b^2}\right) exp\left(\frac{-mz^2}{c^2}\right) \tag{1}$$

and the equation for the rear part of the ellipsoid is:

$$Q_f(x, y, z) = \frac{6\sqrt{3}f_r Q}{abC_r\pi\sqrt{\pi}} exp\left(\frac{-kx^2}{a^2}\right) exp\left(\frac{-ly^2}{b^2}\right) exp\left(\frac{-mz^2}{c^2}\right) \tag{2}$$

where Q_f, Q_r is the heat flux in the front and rear part of the model respectively, Q is the total power, a, b, c_f, and c_r are the width, depth, and length of the front and rear part of the estimated pool, and f_f, f_r are constants which influence energy flow intensity into the material.

A conical source model is usually used when the welding processes are characterized by high energy densities, i.e., laser, electron beam, and plasma welding. Mathematically, the 3D conical heat source model is described in flowing equations:

$$q(x, y, z) = q_0 exp\left(\frac{x^2 + y^2}{r_0^2(z)}\right) \tag{3}$$

$$r_0^2(z) = r_e + \frac{r_i - r_e}{z_i - z_e}(z - z_e) \tag{4}$$

where q_0 is the heat flux density, r_e, r_i are the 3D cone radius dimensions parameters, and z_e, z_i are the 3D cone length parameters.
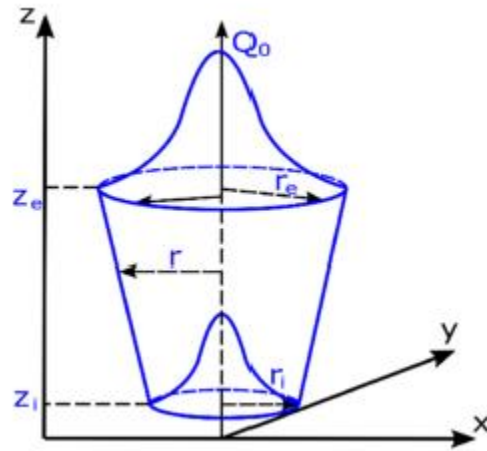
Figure 2. 3D conical heat source model (Kik and Górka 2019).

The most used heat distribution model is Gaussian distribution. It is a model where heat is generated over a surface making it suitable for the numerical modeling of the thin plates (Teixeira, Araújo, and Cunda 2014). The electric arc is modeled in the numerical analysis as a type of surface

heat flux with a Gaussian distribution. The mathematical form of the Gaussian distribution is given below (J. Cho and Na 2009).

$$q_A(x, y) = \frac{VI}{2\pi r_A^2} exp\left(-\frac{x^2 + y^2}{2r_A^2}\right) \tag{5}$$

where, V and I are the voltage and current of the arc, respectively, and r_A is the fixed effective radius of the arc. The equation is a two-dimensional function in the x-axis and y-axis meaning its shape remains unchanged along the z-axis. Also, it shows that the heat flux given by the arc is dependent on the supplied voltage and current, and the effective radius of the arc.

Tungsten Inert Gas Welding

Tungsten Inert Gas (TIG) welding which is also known as Gas Tungsten Arc Welding (GTAW) is an arc-based welding process that uses a non-consumable tungsten electrode, filler metal, and inert gas shield to produce a weld. Gas Metal Arc Welding (GMAW) and Gas Tungsten Arc Welding (GTAW) are the two most used welding processes in the manufacturing processes (Hasanniah and Movahedi 2018). Autogenous TIG welding is a type of welding without the use of filler metal which can be applied for thin sections. In TIG welding the arc is formed between an inert shield of argon or helium and a tungsten electrode. The arc produced in TIG is small and intense enabling for high precision and quality welding. TIG welding technique is hugely popular in welding of the sheet, plate, tube, and casting for use in aerospace, automobile, nuclear, power generation, and other similar industries. TIG welding produces no slag which does not require any flux for this process. TIG also produces little smoke or fumes and does not have any sparks or spatter which makes it suitable for different kinds of welding. TIG welding welds more metals and alloys than any other arc welding process and is good for welding dissimilar metals together. TIG

can be used to weld steel, chromoly, aluminum, nickel alloys, magnesium, bronze, copper, brass, and even gold. Another main advantage of TIG weld is that it can be made in all positions – flat, horizontal, vertical, and overhead. Compared to other arc-welding processes like stick welding, few smoke or fumes are produced in GTAW welding. Slower travel speeds, lower deposition rate, brighter UV rays, and higher equipment costs are some disadvantages of TIG welding.
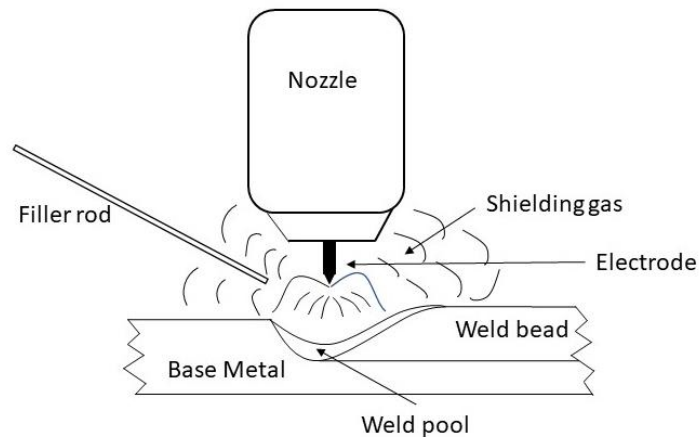
Figure 3. Schematic of TIG welding.

The important process parameters for TIG welding are welding current, voltage, travel speed, wire feeding rate, and shielding gas flow rate (K.H. Tseng 2013). In TIG, these process parameters greatly affect the weld pool geometry which is the weld bead depth and width (Juang and Tarng 2002). Also, it has been seen that the torch angle in TIG welding affects the current density and weld cross-section area. It has been observed that the weld cross-section is nonsymmetric when using 70° and symmetrical in the case of torch angle 90^0 (Parvez et al. 2013). The proper selection of these welding parameters also plays an important role in increasing the weld bead penetration and improving the weld quality. The main disadvantage of TIG welding is its weak penetration and low deposition rate (K.H. Tseng and Hsu 2011). The depth of penetration

in TIG welding is least compared to few other welding processes like Electron Beam Welding (EBM), Laser Beam Welding (LBM), Gas Metal Arc Welding (GMAW), Flux Cored Arc Welding (FCAW), and Submerged Arc Welding (SAW) (A.K. Singh, Dey, and Rai 2017).

Wire Arc Additive Manufacturing

Wire arc additive manufacturing is a branch of additive manufacturing which uses feed wire and electric arc as a fusion source to build 3D metal parts in a layer-by-layer approach. WAAM is an electric arc based direct energy deposition system which uses an electric arc to melt the wire. Wire arc additive manufacturing is becoming more popular in industry and academia due to its ability to create complex 3D parts, less build time, high deposition rate, and environmental friendliness. Also, WAAM offers significant cost savings compared to powder and alternative fusion sources, such as laser and electron beam, respectively. Its ability to produce very net shape preforms without the need for complex tooling, molds or dies offers a significant cost and lead time reductions. WAAM process only deposits the material it needs during the welding process resulting reduced material waster compared to other direct energy deposition process like powder bed fusion where, the full build platform has to be filled with powder. It is also experimentally shown that the WAAM technology, regardless of welding technology used, achieves high quality parts with high deposition rates in stainless steel and titanium alloy (Paskual, Álvarez, and Suárez 2018). But to achieve the desired mechanical requirements it is necessary to choose the correct welding process depending on the material and application required. In contrast, due to the high temperature of the heat source, the material develop high residual stress, undesirable microstructures, and solute segregation and phase transformations at solidification (Cunningham et al. 2018). One of the main disadvantages of the WAAM process is low build resolution. Parts produced from WAAM are lower in resolution with a poor surface finish which would require a

post machining. This secondary processing such as machining and aqua blasting adds more time and cost.
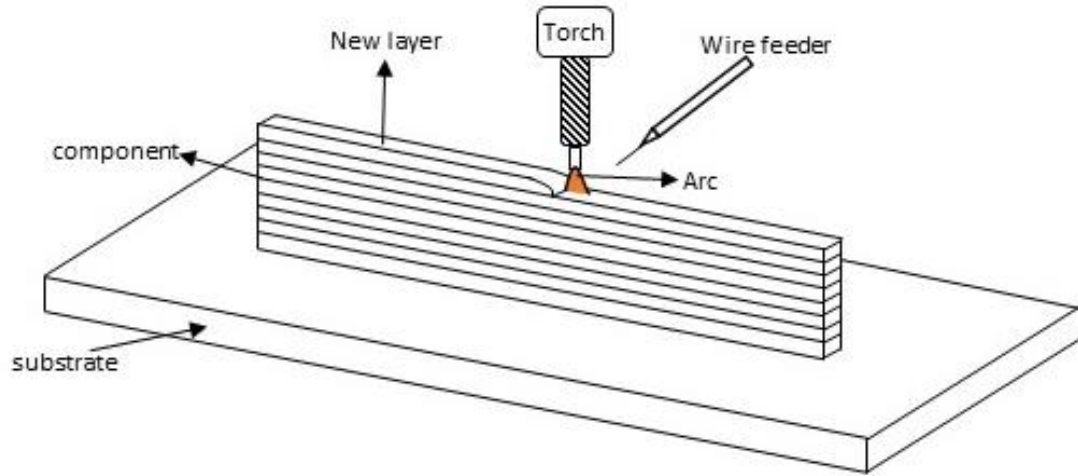
Figure 4. Wire Arc Additive Manufacturing.

Hot-wire arc additive manufacturing combines a preheated filler wire contacting a base metal in a puddle created by tungsten arc of low power density. It is a promising process to fabricate large-scale integral 3D components. An important advantage of hot-wire process is that it can deposit material at high rates using low heat input (Nie et al. 2016). The filler metal is heated by the resistive heat given from the current source. When gas tungsten arc is established, the wire fed current loop is closed and the current flowing through the wire generates the resistance heat in the wire (Chen et al. 2012). The resistance heat produced heats up the wire which is directly proportional to the wire diameter and length of the wire.

$$P = I_w{}^2 R_w \tag{6}$$

$$R_w = \frac{\rho l}{\pi r^2} \tag{7}$$

where P is the power of resistance heat, I_w is the current passing through the wire, R_w is the resistance of the wire, ρ is the electrical resistivity of the wire, l is the length of the wire, and r is the radius of the wire. The heated hot-wire thus can easily melt in weld pool because of preheating achieving high feeding rates and high deposition rates (Spaniol et al. 2020).

Shielding Gas

In TIG welding, the atmospheric gases can react with the weld pool and cause contamination. Thus, a shield is required for this purpose which is provided by the inert shielding gases. Apart from the protection of the weld pool from the atmospheric gases, the shielding gas also influences the heat inputs and arc starting characteristics in TIG welding. Shielding gas is an important parameter of WAAM because it plays a significant role in material quality, properties, and defects (B. Wu et al. 2018). The correct kind and quantity of shielding gas is essential for protecting the weld metal during heating, liquation, and solidification. An inadequate coverage of the arc leads to porosity and excess spatter development (Ley et al. 2015). Conversely, too high flow rate of shielding gas can lead to poor penetration and porosity in the final weld. Each kind of shielding gas has its own thermal, physical, and chemical properties which makes it suitable for different WAAM processes. The weld pool depth can be increased by using shielding gases with high specific heat, thermal conductivity, and viscosity (A.B. Murphy, Tanaka, Yamamoto, et al. 2009).

The three most common shielding gases used for GTAW are 100 percent argon, 100 percent helium and an argon/helium mix. Argon and helium are inert gases while hydrogen, oxygen, carbon dioxide, and nitrogen are the semi-inert gases used in welding. Argon is the most used shielding gas because of its low cost, availability, inertness, and arc starting characteristics. Argon has low ionization potential thus produces high frequency arc starts and stable arc compared

to that of helium. On the other hand, helium has higher thermal conductivity than argon, which helps to produce higher heat inputs. The higher heat input results in faster travel speeds and is good for welding thicker metals because it gives a higher depth-to-width ratio. Helium, unlike argon has higher ionization potential which results in inconsistent arc starts. An argon-helium mixture is used to get the higher heat inputs and superior arc starts. The shielding gas comparison is done in Table 1 (Electric 2008).

Table 1. Shielding gas Comparison (Electric 2008).

CHARACTERISTICS	ARGON	ARGON/HELIUM MIXES	HELIUM
Travel speed	Reduced travel speeds	Improved travel speeds over 100% Argon	Faster travel speeds
Penetration	Reduced penetration	Improved penetration over 100% Argon	Increased penetration
Cleaning	Good cleaning action	Cleaning properties closer to Argon	Less cleaning action
Arc Starting	Easier arc starting	Improved arc starting over 100% Helium	Difficult arc starting
Arc Stability	Good arc stability	Improved arc stability over 100% Helium	Less low amperage stability
Arc Cone	Focused arc cone	Arc cone shape more focused than w/Helium	Flared arc cone
Arc Voltage	Lower arc voltages	Arc voltages between 100% Argon and Helium	Higher arc voltages
Flow Rate	Lower flow rates 10-30 CFH	Higher flow rates than Argon	Higher flow rates (2 times)
Cost	Lower cost and greater availability	Costs higher than Argon	Higher cost than Argon

The shielding gas in the case of WAAM is determined by considering all these factors: application, cost, required heat, and high frequency arc starts. The properties of the tungsten inert gas (TIG) arc are strongly dependent on shield gas. The argon arc has the lowest voltage and lowest maximum arc temperature which results less penetration and small width of the weld (A. Murphy, Tanaka, Tashiro, et al. 2009). Other shielding gases and gas mixtures are expected to increase the weld bead depth and width than a pure argon. It is found out that the addition of other shielding gas (nitrogen, helium, hydrogen) in argon shielding gas increases the arc and arc temperature (Tanaka et al. 2008). The addition of hydrogen to the argon shielding gas increases the weld bead size and shape by influencing the heat generating process in the arc and not by disturbing the fluid flow through Marangoni flow behavior (Onsoien et al. 1995). The reason for this is helium has lower electrical conductivity and nitrogen and hydrogen have higher specific heat. Also, the nitrogen shielded welding on stainless steel has minimal effects on weld hardness but improves the toughness (Keskitalo et al. 2015). It is also considered that nitrogen molecules in the shielding gas are dissociated and turn into nitrogen atoms in the plasma region in the arc welding process (Kodama et al. 2013).

The physical properties of shielding gas play a major role in the welding process. Nitrogen starts dissociating at around 4000 K temperature and completely dissociate in about 10000K temperature. It has been studied and shown that a small quantity of secondary shielding gas in a primary gas mixture can make a significant difference in weld pool dynamics. The physical properties of argon and nitrogen are compared in Figure 5 (a) and (b) (Lias et al. 2018). Nitrogen has higher thermal conductivity and higher specific heat than argon. The high thermal conductivity of nitrogen helps to conduct the heat easily and the high specific heat helps to increase the heat of the system.

(a)   (b)
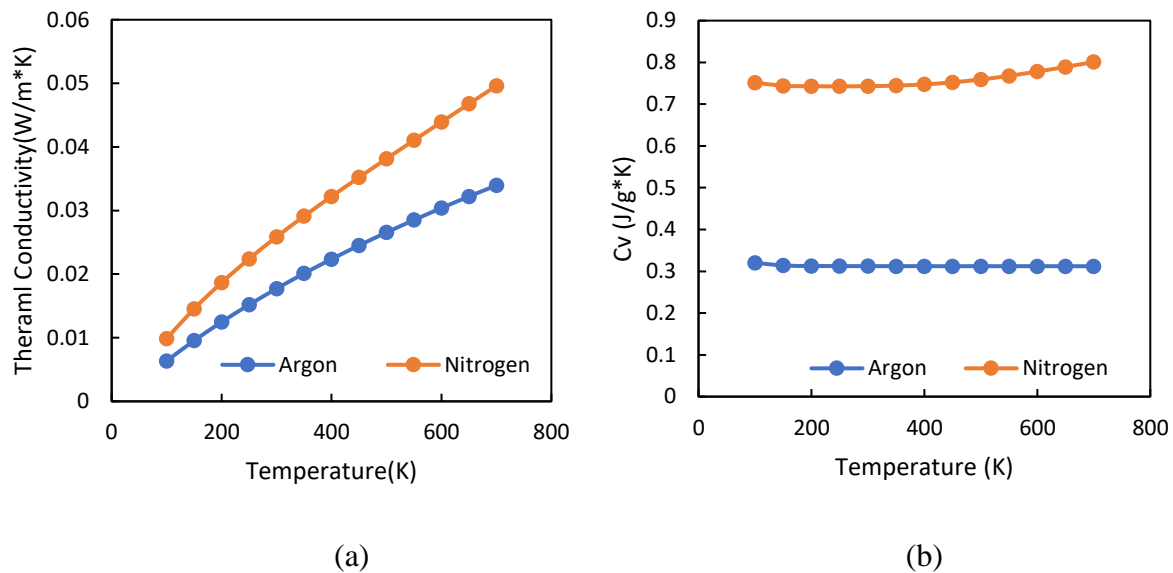
Figure 5. (a) Change of thermal conductivity with temperature (b) change of specific heat with temperature (Lias et al. 2018).

Machine Learning

Machine learning is a process of teaching a computer system to make accurate predictions of the given data. Generally, in machine learning, a known data is given to the computer which does the learning on the data with a specific model and gives the prediction output based on that learning method. The process of learning begins with the known data and the machine makes better decisions in the future based on the provided data. Machine learning uses the knowledge of statistics to find a particular pattern in the input data. Machine learning algorithms has been used as a practical software for computer vision, natural language processing, speech recognition, robot control, and other applications (Jordan and Mitchell 2015). The field of machine learning is growing in welding science as it helps to predict the future result and performs an accurate prediction of the weld. The sophisticated machine learning methodologies, i.e. Gaussian process regression (GPR), support vector machines (SVM), and multi-linear regression (MLR) were used to evaluate the friction stir welding process (Verma, Gupta, and Misra 2018). The use of SVM is

also seen in the detection and classification of the defect and non-defective features of the weld (Wang et al. 2008). The correlation between the friction stir welding (FSW) parameters of aluminum plates and mechanical properties were seen using an artificial neural network (Okuyucu, Kurt, and Arcaklioglu 2007). The model thus developed can be used to calculate the mechanical properties of the weld metal. Similarly, a SVM algorithm was used to identify good and defect weld using extraction of weld image (Ranjan et al. 2016). The prediction of weld quality in high frequency electric resistance welding was carried out using an image processing algorithm (Kim et al. 2007). The weld quality was predicted by using a vision sensor to obtain image of the welding spot. All these and other research works summarize the usefulness of machine learning in the welding process to forecast and monitor the future welds.

Machine learning is used to produce correct outputs for a large sample of inputs and suitably constrain the relationship between the input and the output. Also, it helps to find out the hidden relationships and correlation between large samples of data. The field of machine learning can be organized around three primary areas; task-oriented studies, cognitive simulation, and theoretical analysis (Ayodele 2010). The development of learning systems oriented towards solving a predetermined task is task-oriented studies while a simulation of human learning processes is a cognitive simulation. Machine learning is briefly classified into two parts: a supervised learning method and an unsupervised learning method. Unsupervised learning method fits a model to observations and there is not any specific output. In the case of supervised learning, it learns a function from training data and predicts the output based on the learning algorithm (Shalev-Shwartz and Ben-David 2014).

Supervised machine learning algorithms

Supervised machine learning algorithms model dependencies between the target prediction output and the input feature such that output values for new data are predicted based on relationships that it learned from the previous input data sets. The main aim of the supervised machine learning algorithm is to categorize data from the previous information (A. Singh, Thakur, and Sharma 2016). Supervised learning algorithm is a classification technique which is mainly done on two phases. In the first phase, a classification algorithm is applied on the training data sets and then the constructed model is validated against a known data set to measure the model prediction error and accuracy. There are four different supervised machine learning techniques: logic base algorithm, perception-based techniques, statistical learning algorithms, and support vector machines (Kotsiantis, Zaharakis, and Pintelas 2006). The supervised learning algorithm predicts outcomes for unforeseen test data by learning from the labeled training data. Supervised learning is used if some observations can already be labeled according to a known target concept and a rule or function (model) for this assignment should learn from the data (Lieber et al. 2013). Supervised learning maps the function from the input (x) to the output (y).

$$y = f(x)$$

The goal is to approximate the mapping function so well that when there is new input data (x) can predict the output variables (y) for the data. The mapping function in this case are the types of different learning methods and techniques applied on the input data or training data. Based on the task and types of data, different types of supervised learning methods can be implemented. Regression analysis, classification, decision trees, and support vector machines are some of the types of supervised learning methods.

Support Vector Machines

Developed at AT&T Bell Laboratories, support vector machines (SVMs) are one of the most robust prediction methods based on a statistical learning framework. In machine learning support vector machines are supervised learning models that analyze the data for classification and regression analysis. The main aim in SVM is to find the optimal boundary that maximized the separation between the support vectors (Maxwell, Warner, and Fang 2018). An optimum hyper plane in SVM is determined by the generalization of the training data which is then verified by the test data sets. Support vector machines is the most popular technique of supervised machine learning algorithm with successful applications in the field of facial recognition, text categorization and bioinformatics (Do and Fekete 2007).

SVMs were originally constructed to identify a single linear class boundary i.e., a hyperplane but this limitation was solved by assuming that a linear boundary may exist in a higher dimensional feature space. This transformation of linear data into higher dimensional feature space is called the kernel trick. SVMs can efficiently perform nonlinear classification using specific kernel functions, implicitly mapping their inputs into high-dimensional feature spaces. The kernel functions transform the data into a higher dimensional feature space to make it possible to perform the linear separation (Smola and Schölkopf 2004).
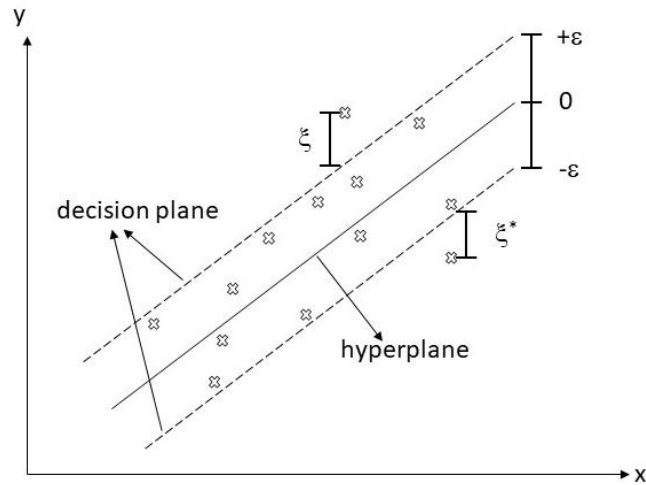
Figure 6. Support Vector Machines.

Suppose the function is,

$$f(x) = <w, x> + b \text{ with } w \in X \text{ and } b \in R \tag{8}$$

where <.,.> denotes dot product in X. Flatness of the above-mentioned function means one must seek the minimum value of w. If there is a hyper plane that exists and satisfies the above equation, the classes are linearly separable. The distance to the closest point is 2/||w||, therefore, the optimum separating hyper plane can be found by minimizing $||w||^2$ under the constraint of Equation 3. Thus, optimum hyper plane is determined by solving the following optimization problem.

$$\frac{1}{2}\|w^2\| + C\sum_{i=1}^{l}(\xi_i + \xi_i^*) \tag{9}$$

subject to constraints

$$y_i - \langle w, x_i \rangle - b \leq \varepsilon + \xi_i \tag{10}$$

$$\langle w, x_i \rangle + b - y_i \leq \varepsilon + \xi_i^* \tag{11}$$

where C is a regularization constant or penalty parameter. The constant $C > 0$ determines the trade-off between the flatness of f and the amount up to which deviations larger than ε are tolerated. The regularization constant allows making a balance between two competing criteria of margin maximization and error minimization (Oommen et al. 2008). The larger value of C means the higher penalty associated with the misclassified samples.

The kernel function in SVM maps the data from linear space to the higher dimensional space. In machine learning, a kernel function is a method of using a linear classifier to solve a non-linear problem. Kernels are generally used to separate the linearly inseparable data. It maps the data into a higher-dimensional space so that it can be linearly separable. Most common kernel functions used in SVMs can be generally divided into four different groups; linear, polynomial, radial basis function, and sigmoid kernels (Kavzoglu and Colkesen 2009). The choice of kernel functions and their parameters hugely influence the performance of the SVM. The kernel function used in the support vector machines was the Gaussian kernel function.

$$k(x_i, x_j) = exp\left(-\frac{\|x_i - x_j\|^2}{2\sigma^2}\right) \tag{12}$$

CHAPTER 3: METHODOLOGY

Mathematical Model

A three-dimensional transient model is used for analyzing the fluid flow and heat transfer of the tungsten inert gas arc welding. Interaction of the metal droplets and weld pool is established with the computational domain. It is assumed that the spherical droplets from a certain fixed height are transferred into the weld pool. The droplets carry the mass, momentum, and energy which is transferred into the weld pool. The initial temperature of the droplet is assumed to be constant. The droplet is also given an initial transfer speed, together with a horizontal speed with the welding torch. The weld pool velocity, temperature, and pressure are calculated by using the conservation of mass, momentum, and continuity (Ribic, Rai, and DebRoy 2008). The fluid is assumed as laminar and Newtonian. The flow is compressible through the buoyancy and Boussinesq approximation. The temperature-dependent fluid density and surface tension coefficient have been used in this simulation (Silwal and Santangelo 2018). The Split Lagrangian (SL) method is used for the volume-of-fluid advection. The momentum advection is the first order, and the time step is controlled by stability and convergence. The viscous stress, heat transfer, surface tension pressure, free surface pressure, and advection solver options are solved explicitly while pressure is solved implicitly. The material properties used in the simulation are given in Table 2. The fluid flow and heat transfer were calculated by the numerical solution of the equations of mass, momentum, and energy in a three-dimensional domain. The governing equations are given as follows.

Table 2. Material Properties used for simulation.

Property	Value
surface tension of pure metal at melting temperature, $(N.m^{-1})$	1.943
melting point of material, (K)	1727
viscosity, $(kg.m^{-1}.s^{-1})$	0.006
specific heat, $(J.kg^{-1}.K^{-1})$	460
thermal conductivity, $(J.m^{-1}.s^{-1}.K^{-1})$	22
liquidus temperature, (K)	1727
solidus temperature, (K)	1670
latent heat of fusion, $(J.kg^{-1})$	2.45×10^5
reference temperature, (K)	1670
contact angle, (degree)	90
saturation pressure, $(N.m^{-2})$	1.01×10^5
saturation temperature, (K)	2843
latent heat of vaporization, $(J.kg^{-1})$	6.34×10^6
specific heat ratio	1.41
accomodation coefficient	0.01
vapor specific heat, $(J.kg^{-1}.K^{-1})$	460
acceleration due to gravity, $(m.s^{-2})$	9.8
coefficient of solidification drag, (s^{-1})	1000
universal gas constant, $(J.Kg\ mol^{-1}.K^{-1})$	8314
droplet frequency (drops/s)	40
infliction point radius (mm)	1.34
droplet radius (mm)	0.445
initial drop temperature (K)	2000
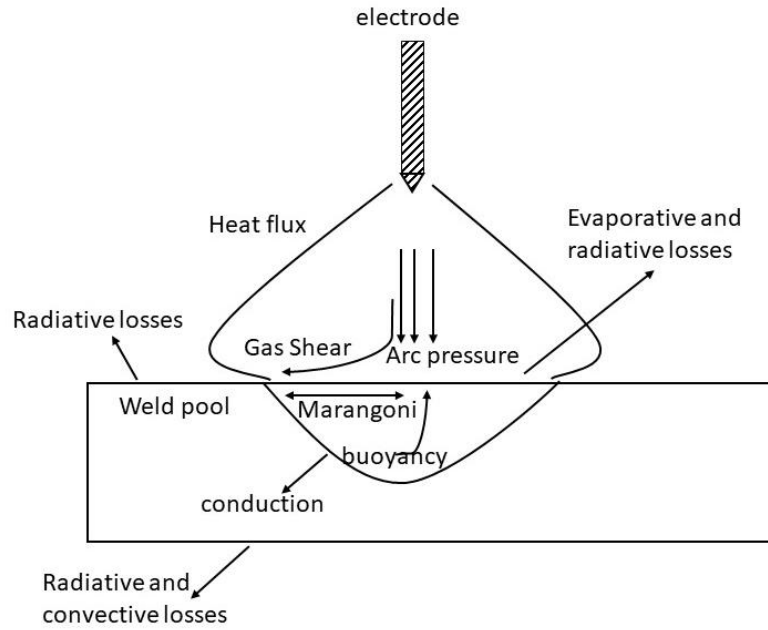
Figure 7. Schematic representation of a gas tungsten welding arc with the weld pool.

Governing equations:

1. Conservation of mass

$$\frac{\partial \rho(T)}{\partial t} + \nabla.\left(\vec{v}\rho(T)\right) = 0 \tag{13}$$

$$\nabla.\vec{v} = 0 \tag{14}$$

where ρ is fluid density and v is the velocity of the fluid.

2. Conservation of momentum

$$\frac{\partial \vec{v}}{\partial t} + \nabla P - \eta\nabla^2\vec{v} + \vec{F} = 0 \tag{15}$$

where P is the hydrodynamic pressure, η is the viscosity and F is the surface and body forces

3. Conservation of energy

$$\frac{1}{\rho(T)}\left[\frac{\partial h}{\partial t} + (\vec{v}.\nabla)h\right] = \nabla.(K\nabla T) \tag{16}$$

where K is the thermal conductivity and h is the enthalpy and given by,

$$h = C_p T + L_f \tag{17}$$

where C_p is the specific heat, T is the temperature, L_f is the latent heat.

4. Volume of fluid (VOF) equation

$$\frac{\partial F}{\partial t} + \nabla.(\vec{v}F) = F_s \tag{18}$$

where F=0 to 1 is the volume fraction of fluid in a cell.

Arc force:

$$F_{arc} = \frac{\mu_o I^2}{8\pi}\left(1 + 2ln\left(\frac{R_2}{R_1}\right)\right) \tag{19}$$

where μ_o is the magnetic permeability of vacuum, I is the welding current, R_1 is the radius of the arc at the welding electrode and R_2 is the radius of the arc at the base metal.

Heat loss equations:

$$K\frac{\partial T}{\partial \vec{n}} + h(T_s - T) + q_{vap} + \sigma\varepsilon(T_s^4 - T^4) = q(r) \tag{20}$$

where, K is the thermal conductivity, n is the normal vector, T_s is the surface temperature, q_{vap} is the heat loss through vaporization, σ is the emissivity, and q(r) is the surface heat flux.

Heat loss through vaporization:

$$q_{vap} = C_{liq}(T - T_l) + L_{vap} \tag{21}$$

where, C_{liq} is the specific heat of the liquid phase and L_{vap} is the latent heat of vaporization.

Electromagnetic Force:

The molten pool of the base metal is subjected to the body forces such as gravity and electromagnetic force. Also, it is subjected to surface forces such as surface tension, Marangoni shear stress due to temperature difference, arc pressure, and arc plasma shear stress (Hu and Tsai 2007). The electromagnetic force in r and z-direction is given in the following equations (Zhou and Tsai 2007):

$$J \times B|_r = -j_r B_\theta, \qquad J \times B|_z = -j_z B_\theta \tag{22}$$

where j_r and j_z are the current density in r and z-direction, respectively. B_θ is the externally applied magnetic flux density whose effect is neglected. According to Ohm's law, the electrical current density in the r and z-direction is given in the equation below.

$$j_r = -\sigma_e \frac{\partial \emptyset}{\partial r}, \qquad j_z = -\sigma_e \frac{\partial \emptyset}{\partial z} \tag{23}$$

where σ_e is the electrical conductivity and ϕ is the electrical potential. It is assumed that the electromagnetic force and arc pressure force are ignored in the numerical model as the impact by the droplet has a higher effect than these body forces.

Pressure due to shielding gases:

$$P_{dynamic} = \rho_{gas} v_{gas}^2 \tag{24}$$

where, ρ_{gas} is the density of the shielding gas and v_{gas} is the velocity of the shielding gas.

Experimental Method

A six-axis FANUC robot with a GTAW torch and argon-nitrogen shielding gases were used in a controlled environment. The tungsten electrode of 3.2m diameter with inconel 625 filler metal and 1018 mild carbon steel were used throughout the experiment. The composition of the base material is given in Table 3 and the composition of filler metal is given in Table 4. Inconel

625 is a nickel-base alloy used mainly for its corrosion resistance and high strength. The primary current level of 160 A was used with a constant distance of 4mm from the base plate to the tungsten. The torch angle was kept at 75^0. The experimental setup is shown in Figure 8. A Phantom VEO-E 310 L high-speed camera is used to capture the arc welding process. The arc and droplet diameter, droplet velocity, and the time interval between each drop are measured from the high-speed footage captured from the camera with a phantom PCC viewer. A micro-epsilon infrared thermometer is used to measure the temperature at the top of the surface of the base metal while a thermocouple is used to measure the temperature at the bottom of the base metal. Two different Omega FMA 5400A/5500A mass flow controllers are used to control the argon and nitrogen shielding gases. The gases from the flowmeter are sent through the static mixture to the weld. The welding parameters are given in Table 5.

Table 3. Chemical composition of base metal weight (%).

Element	Iron, Fe	Carbon, C	Manganese, Mn	Sulfur, S	Phosphorous, P
Content (%)	98.81 - 99.26	0.14 - 0.20	0.60 - 0.90	≤ 0.040	≤ 0.050

Table 4. Chemical composition of filler metal weight (%).

	Cr	Ni	Mo	Co	Cb+Ta	Al	Ti	C	Fe	Mn	Si	P	S
MIN	20	–	8	–	3.15	–	–	–	–	–	–	–	–
MAX	23	balance	10	1	4.15	0.4	0.4	0.1	5	0.5	0.5	0.015	0.015

Table 5. Welding Parameters.

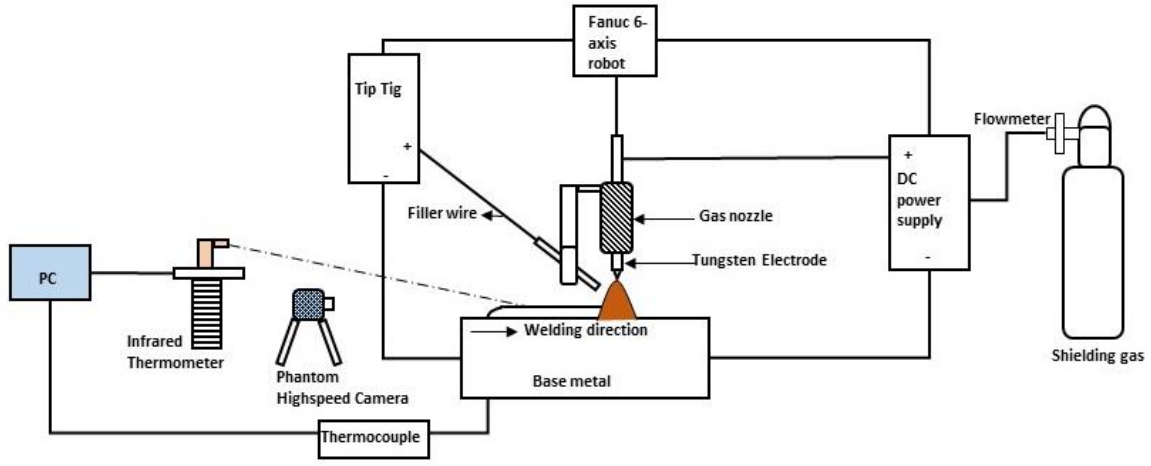| Parameters	Values
Primary current (A)	160
Travel speed (mm/s)	5
Wire-fed speed (mm/s)	35
Welding wire diameter (mm)	0.9
Tungsten diameter (mm)	3.175

Figure 8. A schematic of an experimental setup.

Experiment data were collected for three different flowrates, 8 lpm (16.95 cfh), 10lpm (21.19 cfh), and 13 lpm (27.55 cfh). For each flowrate, the nitrogen and argon shielding gases are changed and the experiment is carried out keeping all the other variables constant.

Machine Learning Algorithm

A support vector machines with a Gaussian kernel was used to do the regression analysis. Out of the total 35 data collected for the 8 lpm flowrate of shielding gases, the data was divided into two parts: 70 percentage used for training and 30 percentage for testing using cross-validation. Support vector machines algorithm with Gaussian kernel function was used to do the model analysis on the training data and prediction was done on the testing data. Also, SVM with polynomial and linear kernel, linear, Gaussian process, and regression tree models was used to compare the model loss in each regression analysis technique.
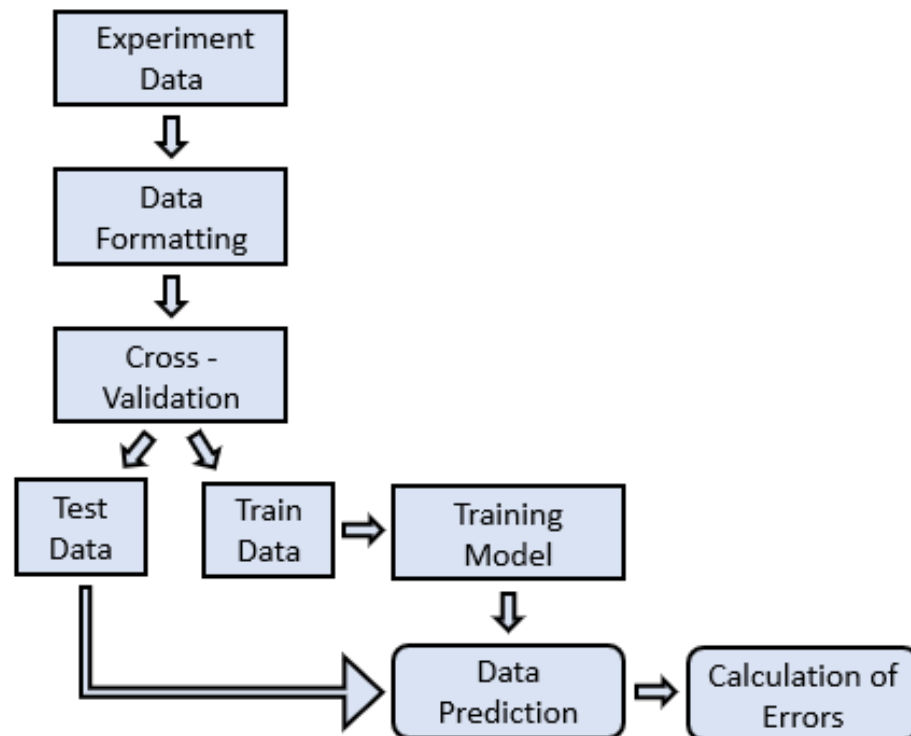
Figure 9. Flow of machine learning process.

Figure 9 shows the flow of the process of data prediction. The collected experiment data was formatted, and any outliers present in the data were removed. The removal of the outliers helps

to carry out the process effectively. After the data formatting, a cross-validation process was applied to separate the data into two different groups: test data and training data. Training data consists of 70% of the total experiment data while test data consists of 30% of the total data collected. After cross-validation a training model was executed on the training data. The training model is SVM regression model using Gaussian kernel. The training model was then used to predict the future result based on the predictive variables on test data. The predicted value was compared with the original value of test data to calculate the predictive loss, similarities, deviation, and mean standard error. Different logical graphs and figures were plotted to analyze the predictive responses with the actual responses.

CHAPTER 4: RESULTS AND DISCUSSION

Heat flux and electrode arc analysis

Heat flux in the simulation is the major variable that changes the weld bead depth and width extensively. So, the calculation of the heat flux should be accurate and should be approximated closely to get good results on the simulation. To calculate the heat flux, the power of the dc supply is used with 60% efficiency for the TIG welding. The required heat flux is calculated using the following equation (Ribic, Rai, and DebRoy 2008).

$$q = \eta \frac{q_f}{2\pi\sigma} exp \left\{ - \left(\frac{r}{\sigma} \right)^2 \right\} \tag{25}$$

where q_f is the power of the DC welder, r is the radius, η is the efficiency of TIG welding, and σ is the heat distribution parameter usually taken as the radius of the arc. Argon shielding gas was used with the electrode offset distance of 4 mm. The arc diameter is measured from the high-speed footage of the welding. Figure 10 shows the picture taken of the tungsten arc using Phantom VEO-E 310 L high-speed camera. The known quantity in the picture is the diameter of the filler which is 0.9 mm. Based on the known quantity, the diameter of the arc is measured with the use of Phantom PCC software.

Figure 10. Tungsten arc with the known diameter of filler wire (0.9 mm).

The calculated heat flux is given as the input heat flux into the simulation. Similarly, other quantities measured from the high-speed video analysis of the arc welding is given as input to the simulation. The heat flux distribution is taken as Gaussian in the simulation. The simulation result is then compared with the experimental result. Also, Figure 11 shows the comparison between the tungsten arc for 100% Ar arc and 3% N_2-97% Ar arc. The electrode arc in the case of argon is more stable and the weld pool does not look distorted. Also, the filler wire is melted at a slow rate in the case of argon only arc. Whereas the electrode arc is observed unstable and more spattering is observed in the weld pool in the case of the Ar-N_2 mixture. The measured droplet diameter for Ar only and Ar-N_2 mixture of shielding gas are 1.95 mm and 1.31 mm respectively. Also, the droplet formation time in case of Ar only is 6.7 s while in case of Ar-N_2 mixture it is 1.7 s. The result shows that smaller droplet diameter is formed in case of Ar-N_2 mixture in a high frequency

while comparatively large droplets are formed in case of Ar only shielding gas with low droplet frequency. The high temperature of arc of Ar-N$_2$ arc melts the wire faster resulting the small droplet diameter and high frequency.

Figure 11. Comparison of 100% argon arc (left) and 3% nitrogen-97% argon shielding gas arc (right).

Comparison of simulation result with the experiment

Figure 12 shows the simulation result for the width and height measurement. The simulation results are similar to the experiment results with the argon shielding gas with an electrode offset of 4 mm from the base plate. The experiment result is also shown in Figure 12. The average depth and width measured for the experiment are 0.252 cm and 0.522 cm respectively which are close to the simulation result. The average percentage errors in the comparison of depth and width of the weld bead are 1% and 2.3% respectively. The minimum error on the comparison shows that the simulation model is close to the experiment. The only difference observed between the simulation and experiment results was the cross-section surface. The cross-section shape of the simulation is symmetrical and concave shape while the cross-section area of the experimental

result is asymmetrical. This is due to the torch angle which is kept at 75^0 in the experiment. The distribution of current density and the heat flux caused by electron contribution is of maximum value behind the arc center in case of 70^0 angle resulting in an asymmetrical shape (Parvez et al. 2013). In the numerical analysis, the torch was kept at 90^0 giving a symmetrical shape.
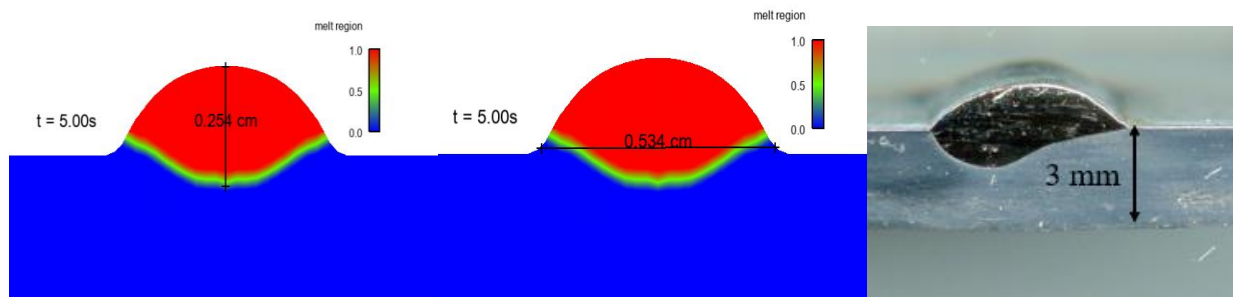

Figure 12. The cross-section profile showing bead shape for HW GTAW compared with the experiment result (right).

It is known that the addition of nitrogen shielding gas in argon shielding gas raises the temperature of the arc and thus the heat flux given by the arc (Tanaka et al. 2008). Also, the addition of other secondary gases like hydrogen and helium performs the same phenomenon. To see the effect of the addition of nitrogen on the Ar-N2 shielding gas, the efficiency of the heat flux was increased by 20 percent and the simulation results were compared with the experimental results. Figure 13 shows the cross-section profile of the simulation results for HW GTAW. The results show an increase in the width and depth of the weld pool because of the increase in the heat flux of the system. The simulation results are similar to the experimental results when 2.25 % of nitrogen is added to the shielding gas mixture. The average depth and width measured for the experiment result are 0.28 cm and 0.55 cm respectively which is also shown in Figure 13. The

velocity distribution is shown in Figure 14 with the directional vectors for the 20% increase in heat flux. It is seen that the velocity is more in case of increased heat flux than the initial low heat flux case. Also, it is seen that the velocity vectors in yz plane are oriented more towards the side and depth in case of increased heat flux. The increase in depth and width thus can also be verified seeing this velocity contour and vector orientation on the simulation result.
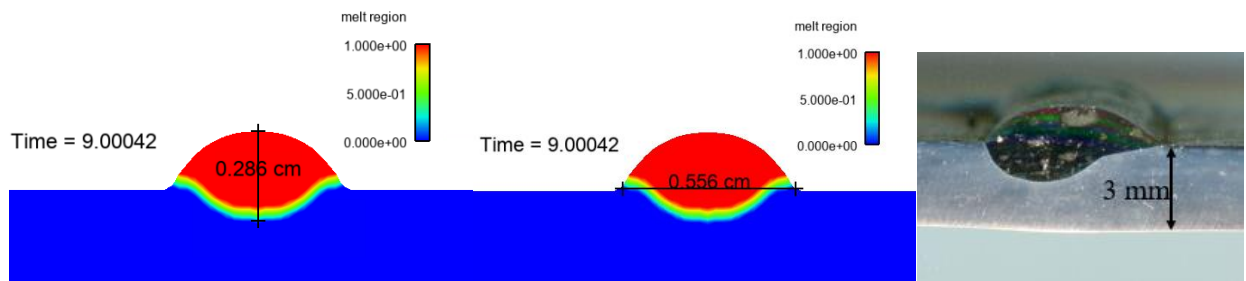
Figure 13. The cross-section profile showing bead shape for HW GTAW with 20% increase in heat flux compared with experiment result (right).
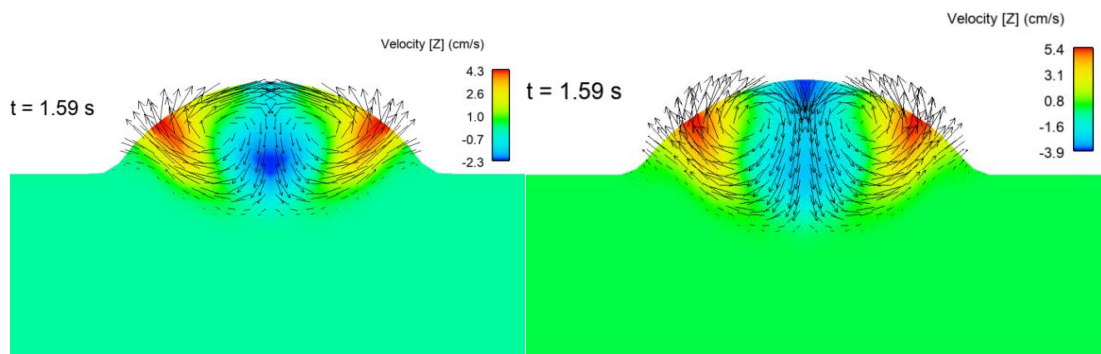
Figure 14. Velocity distribution after 20% increase in heat flux (right) on yz plane.

Effect of addition of N_2 on temperature

The temperature on the top of the base plate is measured using an infrared thermometer as shown in Figure 8. Two different temperature readings were taken for two different shielding gases mixture. 100 % argon shielding gas was used for the first weld while a mixture of 5.26 % nitrogen

and 94.74% argon was used for the second weld. The total flow rate for both cases was maintained at 10 lpm. Figure 15 shows the temperature reading for both cases. The maximum temperature reached in Ar only is 1344.8^{o}C and the maximum temperature reached in a mixture of Ar-N$_2$ is 1396.9^{o}C. It shows that there is an increase in arc temperature when nitrogen is added to the argon shielding gas. The cross-section of the weld is shown in Figure 16. The cross-section of the weld shows the increased depth and width in case of a mixture of 5.26 % nitrogen and 94.74% argon than 100 % argon shielding gas.
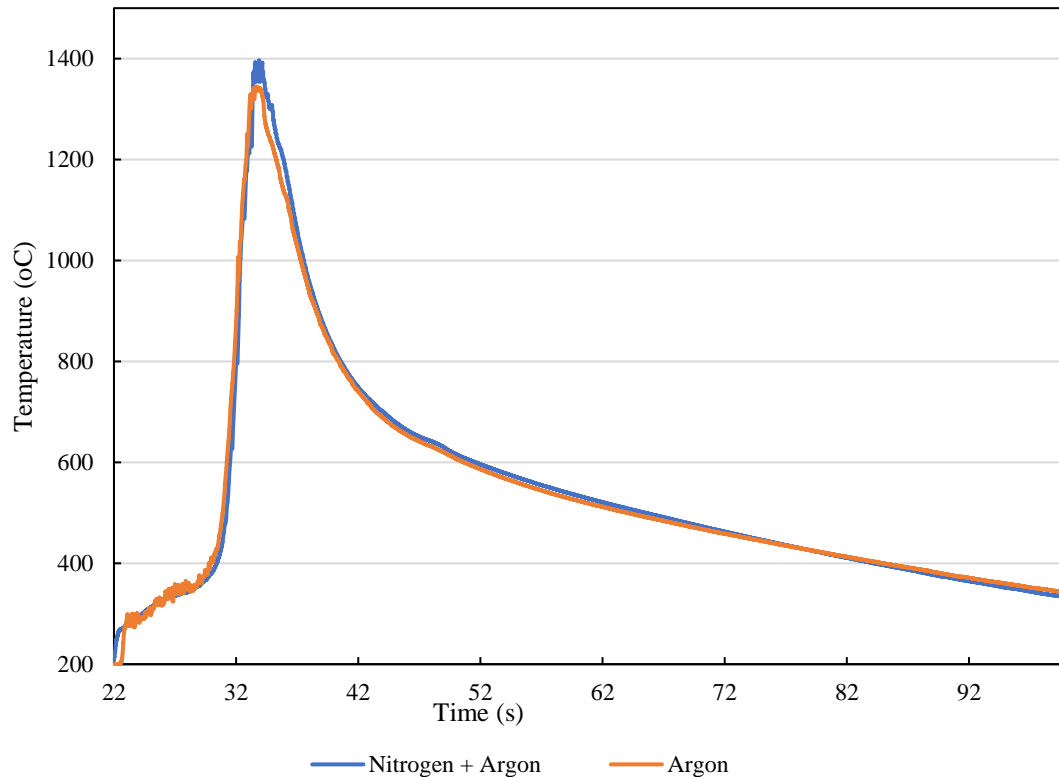
Figure 15. Temperature measurement for two different shielding gas mixture.
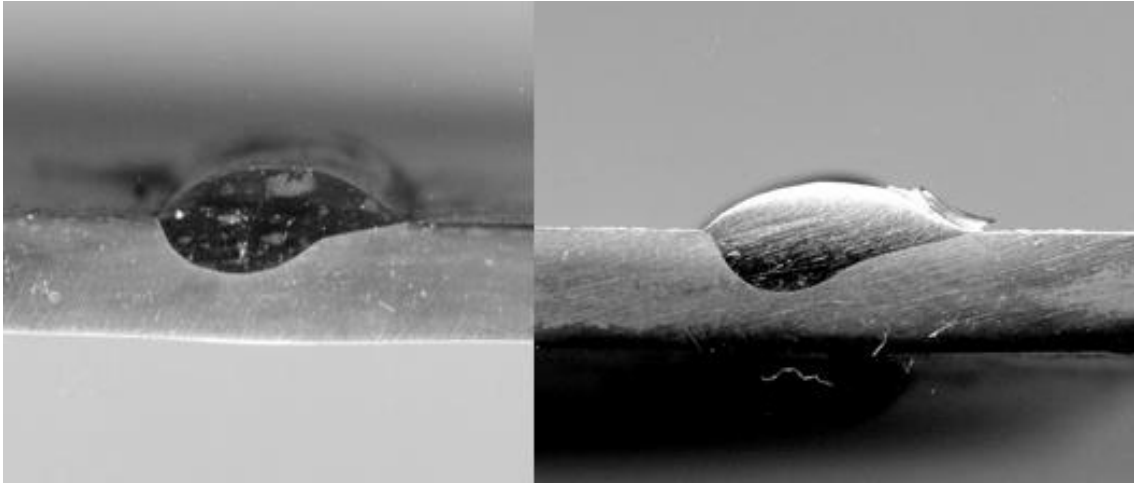
Figure 16. Cross-section of the experiment welds. The left cross-section is for 100% argon shielding gas while the right cross-section is for a mixture of 5.26 % nitrogen and 94.74% argon shielding gases.

The temperature distribution from the simulation result is compared with the experiment result. The experiment with 100% argon shielding gas is used for the comparison. Figure 17 shows the temperature variation with time for the simulation and experiment results. It shows that temperature reached high in case of simulation. There is more heat loss to the atmosphere and welding table in an experiment which constricts it from reaching the high temperature. A better boundary condition for heat loss in the simulation can reduce this temperature difference. The nature of the graph in both cases is the same, the heating and cooling nature of both simulation and experiment results are similar.
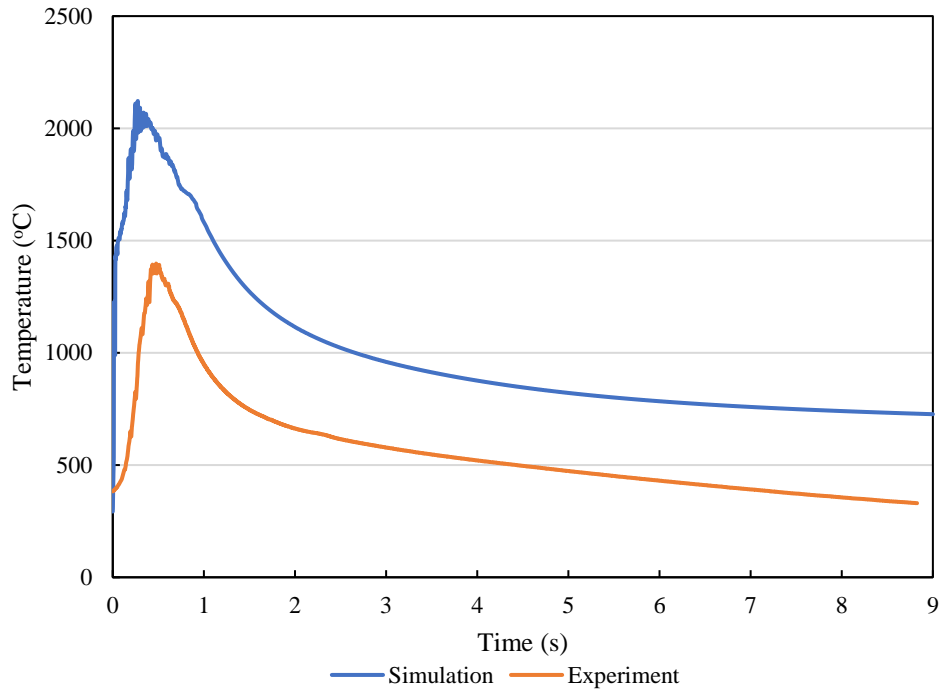
Figure 17. Comparison of temperature distribution in simulation and experiment.

Effect of addition of N_2 in width and depth of weld pool

Figure 18 shows the trend of variation of width and depth with an increase in nitrogen percentage. It shows that there is an increase in the depth and width of the weld pool with the increase in nitrogen percentage in the Ar-N_2 shielding gases mixture. As mentioned before, the increased depth and width of the weld pool is due to the high heat flux due to the addition of nitrogen shielding gas in the mixture.
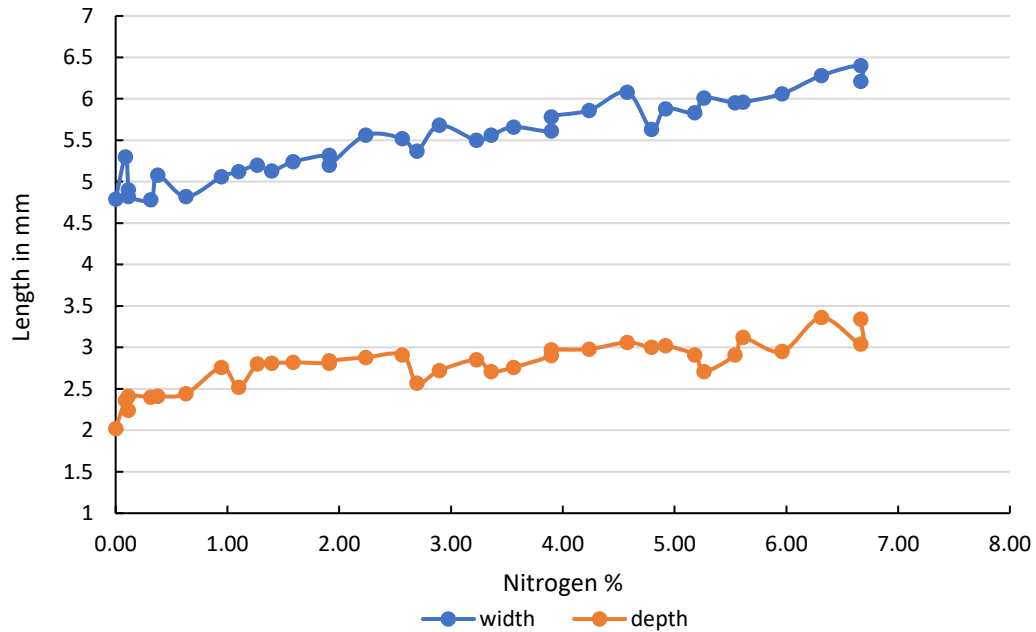
Figure 18. Effect of nitrogen percentage on weld pool depth and width (8lpm).

Also, a similar trend can be seen in the increased flow rate of shielding gases. As seen in Figures 19 and 20, the width and depth of the weld pool both increases with the increase in the percentage of nitrogen in the Ar-N$_2$ shielding gases mixture. Figure 19 shows the effect of nitrogen percentage on the weld bead depth and width for the total flowrate of 10 lpm Ar-N$_2$ shielding gases mixture while Figure 20 shows the same effect for the total flowrate of 13 lpm Ar-N$_2$ shielding gases mixture.
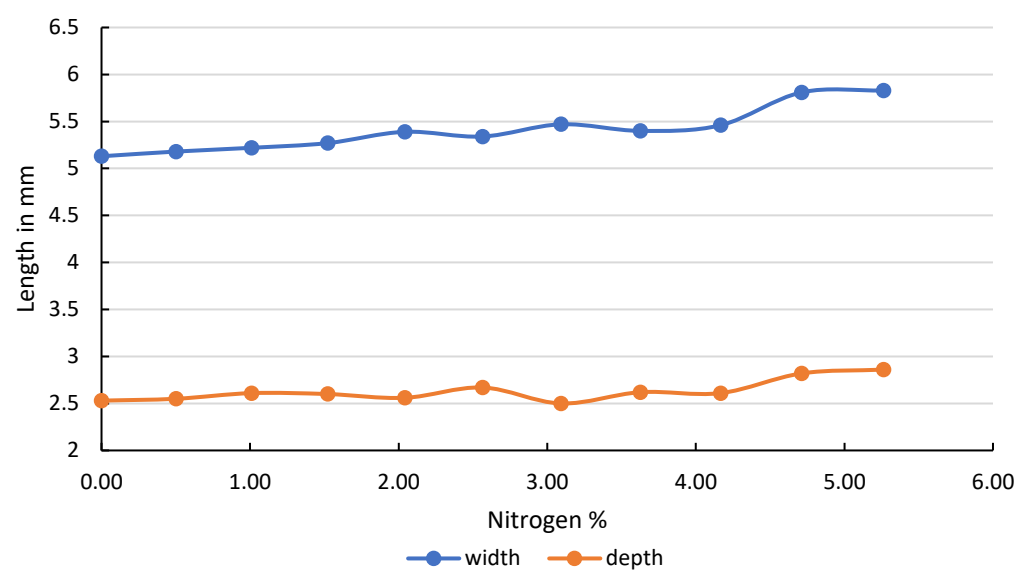
Figure 19. Effect of nitrogen percentage on weld pool depth and width (10lpm).
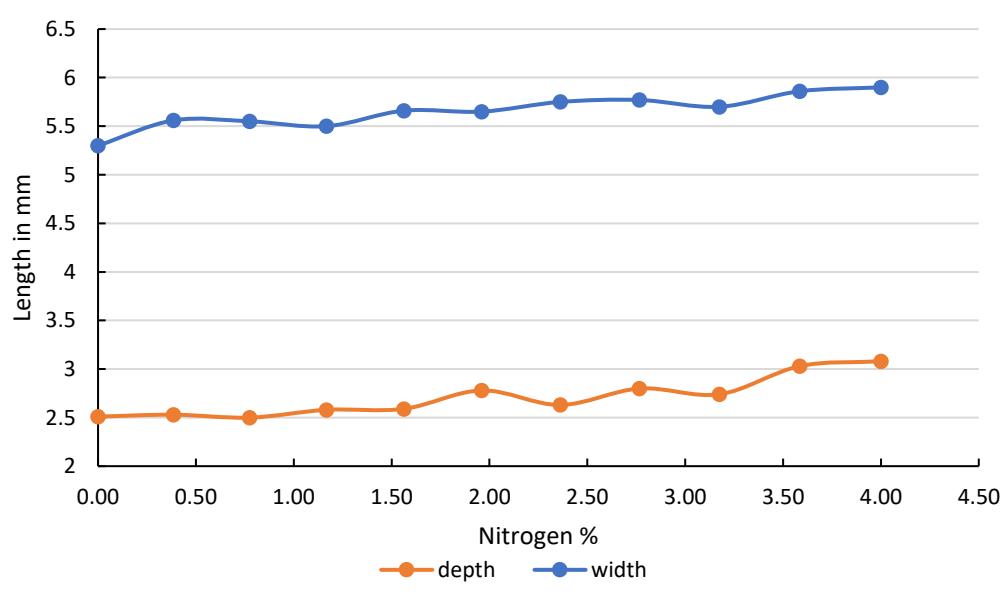
Figure 20. Effect of nitrogen percentage on weld pool depth and width (13lpm).

With the increase in nitrogen percentage in the Ar-N$_2$ shielding gases mixture, spattering and unstable arc are seen. Figure 21 shows the effect of increased nitrogen in shielding gas mixture

externally. The arc was observed unstable and more spattering is seen when the nitrogen flowrate is more than 400ml/min. Also, the formation of soot around the weld bead is seen with the increase of nitrogen flow rate which is due to the formation of nitrogen oxides at high temperature (Thrysin, Gerhardsson, and Forssman 1952).
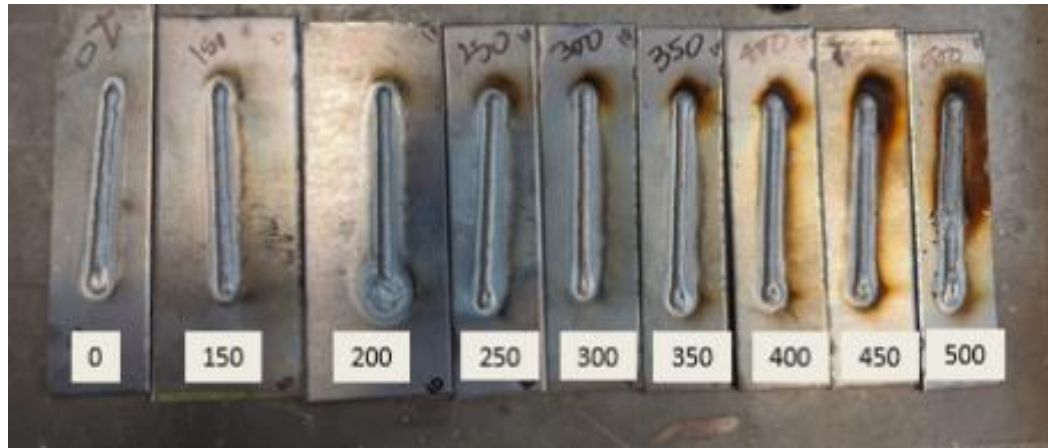
Figure 21. Increment of N_2 form 0-500ml/min in a 10 l/m Ar-N_2 mixture.

Regression Analysis

A Support Vector Machines (SVM) regression analysis with Gaussian kernel is used for the prediction analysis. Table 6 shows the model loss for different regression analysis models. Out of all the used regression analysis model, SVM with Gaussian kernel function has the smallest model loss, that is why it is used for the prediction analysis. The predictive variables used for the regression analysis were nitrogen and argon flowrate while the response variable used was depth/width.

Table 6. Regression models with losses.

Model	Model Error(%)
SVM(Gaussian kernel)	2.24
SVM (Polynomial kernel)	15.31
SVM(Linear Kernel)	5.05
Linear	14.6
Regression Tree	3.56
Gaussian Process	3.15

The depth regression analysis shows the model loss of 2.24% with a mean standard error of 2.236 % and a mean absolute prediction error of 4.654 % as shown in Figure 23 (a) and (b). Figure 22 (a) shows the variation of depth of test data and predicted data with the change of nitrogen percentage. The predicted response is close to the test data which verifies the lesser prediction error. Also, the actual depth is close to the predicted depth shown in Figure 22 (b). An imaginary line at 45 degrees is created to see the variation of actual depth with the predicted depth. Out of a total 10 predicted depth value, 6 data points are very close to the line while rest 4 data points are close as seen in Figure 22 (b) which is the reason for the low mean absolute prediction error of 4.654%.

(a)	(b)

Figure 22. (a) Predicted response vs the test data (b) Actual depth vs predicted depth.

(a)	(b)
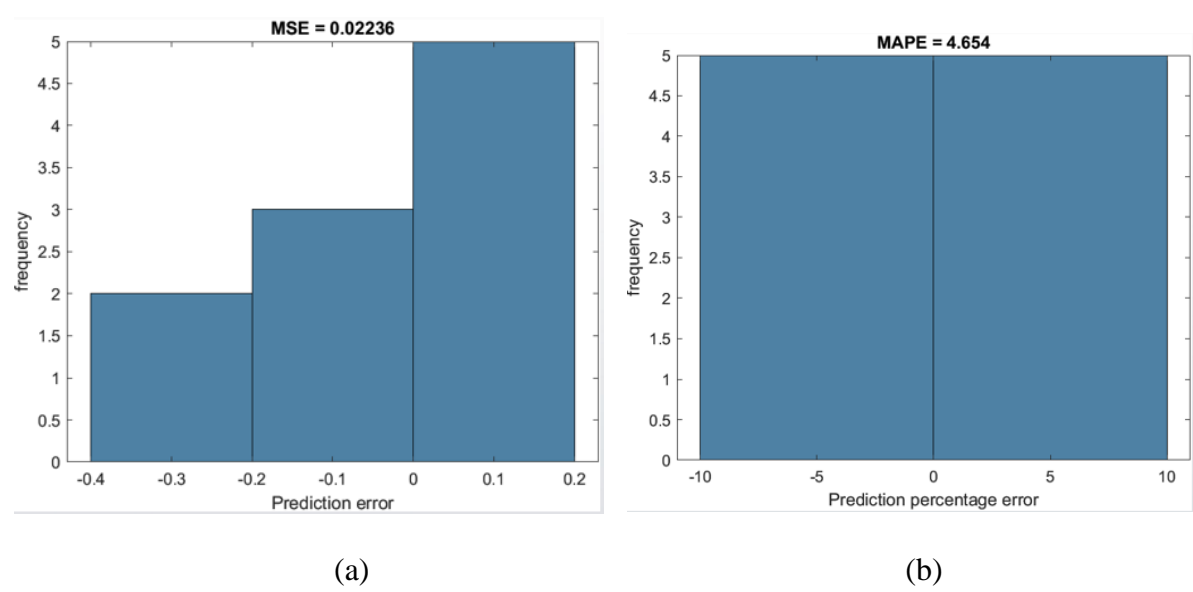
Figure 23. (a) Prediction error in depth analysis (b) Prediction percentage error.

Similarly, the width prediction analysis is also performed which predicts the width for the test data with a mean standard error of 3.4% and a mean prediction error of 2.462 % as shown in Figure 25 (a) and (b) respectively. As like the depth analysis, the width analysis is carried out with width as a response variable and nitrogen - argon shielding gas flowrate as a predictive variable.

Figure 24 (a) shows the test and predicted data for a width prediction with the change in nitrogen percentage. The predicted responses are close to the test data with few of the data points overlapping each other. Further, Figure 24 (b) shows the variation of actual width to the predicted width which verifies the former plot. As most of the predicted width is close to the actual width, the width prediction has a mean prediction error of only 2.462% which is less than the depth prediction discussed before. The higher mean prediction error in case of depth regression analysis indicated the predicted results are more varied in case of depth prediction than the width prediction. The nature of the experiment data collected causes the variation in predicted data. Figure 18 shows the collected data for the depth and width measurement. The figure shows that there is more variation in the depth data than the width data and the trend of graph for depth is more distorted compared to the width measurement. This variation of collected data explains the different mean prediction error for depth and width measurement.

(a)   (b)

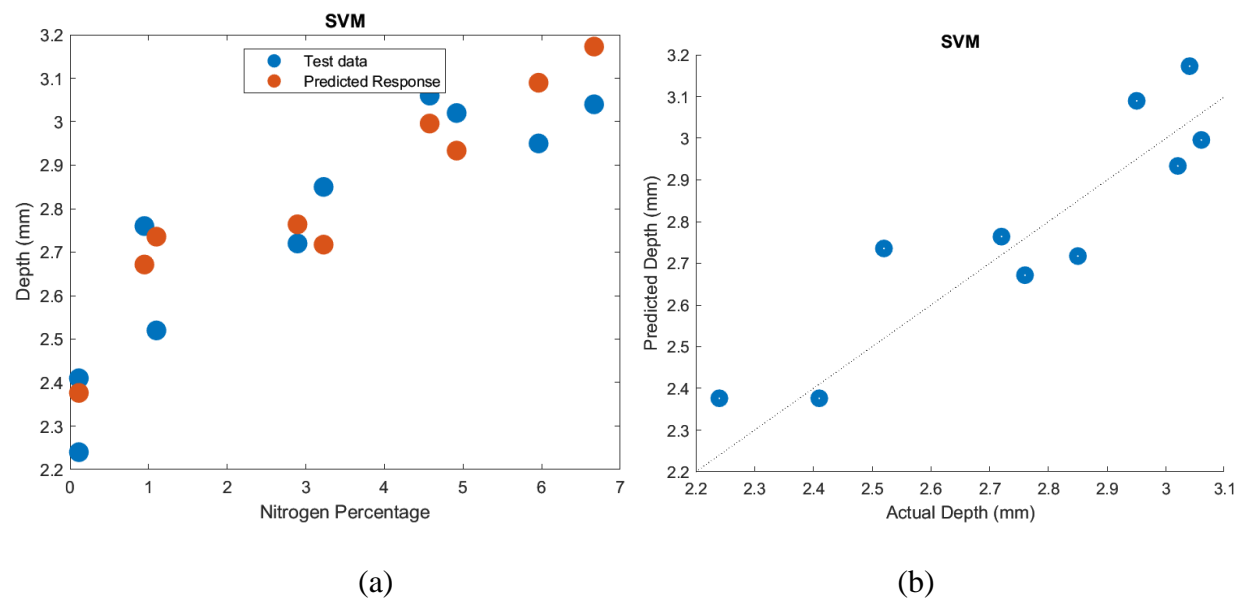Figure 24. (a) Predicted response vs the test data (b) Actual width vs predicted width.
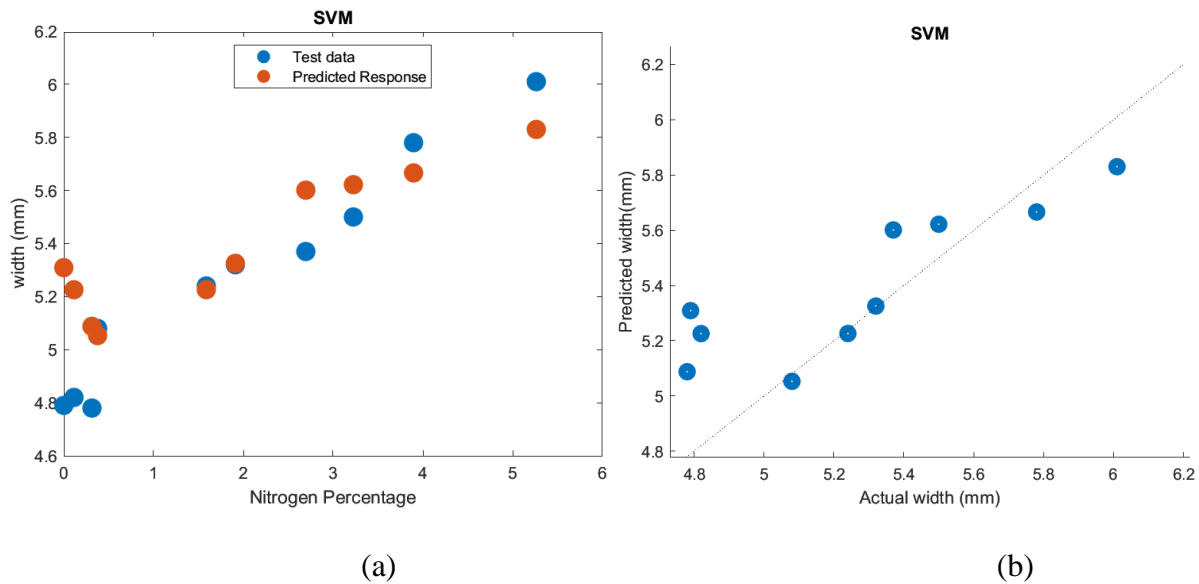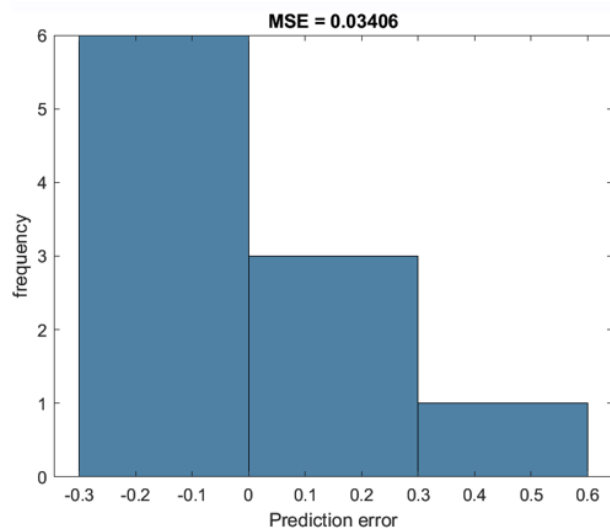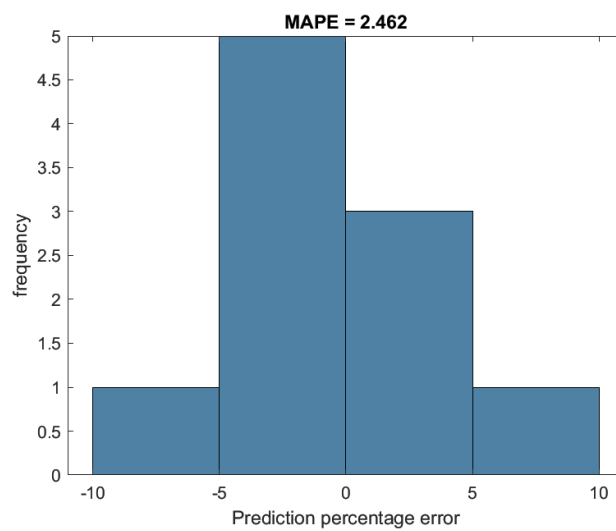
(a)   (b)

Figure 25. (a) Prediction error in depth analysis (b) Prediction percentage error.

CHAPTER 5: CONCLUSIONS AND RECOMMENDATIONS

Conclusions

A numerical and experimental study of the effect of the Ar-N_2 shielding gases on the width and depth of the weld pool was performed. The rise in arc temperature is seen with the addition of the nitrogen shielding gas in the Ar-N_2 shielding gases mixture which increases the depth and width of the weld bead. The simulation result shows good agreement with the experimental results. The following conclusion can be drawn from the study:

1. The experimental result verifies the computational model with similar shape and weld morphology. The depth and width measured from the computational model with an additional 20% increase in heat flux are similar to the experimental result with 2.25% addition of nitrogen in Ar-N_2 shielding gases mixture. The increase in temperature for Ar-N_2 arc verifies the increased depth and width of the weld bead.

2. An increase in the width and height of the weld bead is observed with the increase of nitrogen percentage in the shielding gases mixture. The increase in width and height of the weld bead is due to the increased arc temperature. Nitrogen has higher specific heat compared to argon which helps to increase the temperature of the system.

3. The change in the flowrate of the shielding gas does not have a significant change in depth and width of the weld bead. The depth and width measured for three different flow rates i.e., 8 lpm, 10 lpm and 13 lpm are almost the same which shows no significant change with an increase in the total flow rate of shielding gases.

4. Spattering and an unstable arc are noticed when the nitrogen flow rate is increased beyond 400 ml/min.

5. Prediction of width and height is done with a prediction error of 4.654% and 2.462%. SVM algorithm with Gaussian kernel function has the least model loss compared to other regression analysis. The prediction percentage error is below 4% for the prediction of depth and width, respectively.

Recommendations and Further Research

The accuracy of the computational results depends upon the different factors considered in the numerical model. Numerous factors affect the numerical results which can be improved by considering each force that acts on the GTAW. The experiment results can be made more consistent using a digital flowmeter with precise control. A small increase in the percentage of nitrogen in a mixture of shielding gases has significant impact on the weld. Therefore, precise flowmeter with less tolerance value can solve the problem in the gas flow. Also, the result could be more consistent if the automated grinding of the tungsten electrode is done. Research has shown the grinding process of tungsten can affect the arc produced. As the tungsten was grinded manually, each grinded tungsten varies in the structure. Regression analysis will be more efficient and effective with the use of more data. The following areas are suggested for further research:

1. Effective measurement of arc voltage of the tungsten inert gas welding can be done. As it is known that the addition of N_2 in the Ar-N_2 shielding gases mixture increase the arc voltage, the measurement of voltage in each step helps to calculate the heat flux for the numerical simulation.

2. In the present study, the simulation of the addition of N_2 gas is done by increasing the heat flux by certain percentage. In other way, two shielding gas model can be simulated in the mathematical method to verify the change in temperature and heat flux in the experiment

results. This type of model can give the direct reading of change in heat flux with the change of shielding gas in the system.

3. The use of neural networks and deep learning can be used in the future to predict the future results and compare the results with support vector machines.

REFERENCES

Ayodele, Taiwo Oladipupo. 2010. "Types of machine learning algorithms." *New advances in machine learning* 3: 19-48.

Cao, Z, Z Yang, and XL Chen. 2004. "Three-dimensional simulation of transient GMA weld pool with free surface." *Welding Journal-New York-* 83: 169-S.

Chen, JS, Y Lu, XR Li, and YM Zhang. 2012. "Gas tungsten arc welding using an arcing wire." *Welding Journal* 91 (10): 261-269.

Cho, Dae Won, Woo Hyun Song, Min Hyun Cho, and Suck Joo Na. 2013. "Analysis of submerged arc welding process by three-dimensional computational fluid dynamics simulations." *Journal of Materials Processing Technology* 213 (12): 2278-2291.

Cho, JH, and Suck Joo Na. 2009. "Three-dimensional analysis of molten pool in GMA-laser hybrid welding." *Welding Journal* 88 (2): 35s-43s.

Cunningham, CR, JM Flynn, Alborz Shokrani, Vimal Dhokia, and ST Newman. 2018. "Invited review article: strategies and processes for high quality wire arc additive manufacturing." *Additive Manufacturing* 22: 672-686.

Do, Thanh Nghi, and Jean Daniel Fekete. 2007. "Large scale classification with support vector machine algorithms." Sixth International Conference on Machine Learning and Applications (ICMLA 2007).

Ebrahimnia, Mohamad, Massoud Goodarzi, Meisam Nouri, and Mohsen Sheikhi. 2009. "Study of the effect of shielding gas composition on the mechanical weld properties of steel ST 37-2 in gas metal arc welding." *Materials & Design* 30 (9): 3891-3895.

Electric, Miller. 2008. "Guidelines For Gas Tungsten Arc Welding (GTAW)." *Illinois Tool Works, Co., Appleton, WI*.

Fan, HG, Hai-Lung Tsai, and Suck-Joo Na. 2001. "Heat transfer and fluid flow in a partially or fully penetrated weld pool in gas tungsten arc welding." *International Journal of heat and mass transfer* 44 (2): 417-428.

Harlow, Francis H, and J Eddie Welch. 1965. "Numerical calculation of time-dependent viscous incompressible flow of fluid with free surface." *The physics of fluids* 8 (12): 2182-2189.

Hasanniah, A, and M Movahedi. 2018. "Welding of Al-Mg aluminum alloy to aluminum clad steel sheet using pulsed gas tungsten arc process." *Journal of Manufacturing Processes* 31: 494-501.

Heiple, CR, JR Roper, RT Stagner, and RJ Aden. 1983. "Surface active element effects on the shape of GTA, laser and electron beam welds." *Weld. J.* 62 (3): 72.

Hu, J, and Hai Lung Tsai. 2007. "Heat and mass transfer in gas metal arc welding. Part I: The arc." *International Journal of Heat and Mass Transfer* 50 (5-6): 833-846.

Huang, Her Yueh. 2009. "Effects of shielding gas composition and activating flux on GTAW weldments." *Materials & Design* 30 (7): 2404-2409.

---. 2010. "Argon-hydrogen shielding gas mixtures for activating flux-assisted gas tungsten arc welding." *Metallurgical and Materials Transactions A* 41 (11): 2829-2835.

Jordan, Michael I, and Tom M Mitchell. 2015. "Machine learning: Trends, perspectives, and prospects." *Science* 349 (6245): 255-260.

Juang, SC, and YS Tarng. 2002. "Process parameter selection for optimizing the weld pool geometry in the tungsten inert gas welding of stainless steel." *Journal of materials processing technology* 122 (1): 33-37.

Kavzoglu, Taskin, and Ismail Colkesen. 2009. "A kernel functions analysis for support vector machines for land cover classification." *International Journal of Applied Earth Observation and Geoinformation* 11 (5): 352-359.

Keskitalo, M, K Mäntyjärvi, Jesper Sundqvist, John Powell, and AFH Kaplan. 2015. "Laser welding of duplex stainless steel with nitrogen as shielding gas." *Journal of Materials Processing Technology* 216: 381-384.

Kik, Tomasz. 2020. "Heat Source Models in Numerical Simulations of Laser Welding." *Materials* 13 (11): 2653.

Kik, Tomasz, and Jacek Górka. 2019. "Numerical simulations of laser and hybrid S700MC T-joint welding." *Materials* 12 (3): 516.

Kim, D, T Kim, YW Park, K Sung, M Kang, C Kim, C Lee, and S Rhee. 2007. "Estimation of weld quality in high-frequency electric resistance welding with image processing." *Welding Journal-New York-* 86 (3): 71.

Kodama, S, K Sugiura, S Nakanishi, Y Tsujimur, M Tanaka, and AB Murphy. 2013. "Effect of plasma heat source characteristics on nitrogen absorption in gas tungsten arc weld metal." *Welding in the World* 57 (6): 925-932.

Kotsiantis, Sotiris B, Ioannis D Zaharakis, and Panayiotis E Pintelas. 2006. "Machine learning: a review of classification and combining techniques." *Artificial Intelligence Review* 26 (3): 159-190.

Kshirsagar, Rohit, Steve Jones, Jonathan Lawrence, and Jim Tabor. 2019. "Prediction of Bead Geometry Using a Two-Stage SVM–ANN Algorithm for Automated Tungsten Inert Gas (TIG) Welds." *Journal of Manufacturing and Materials Processing* 3 (2): 39.

Ley, FH, SW Campbell, AM Galloway, and NA McPherson. 2015. "Effect of shielding gas parameters on weld metal thermal properties in gas metal arc welding." *The International Journal of Advanced Manufacturing Technology* 80 (5-8): 1213-1221.

Liang, Rong, Rui Yu, Yu Luo, and YuMing Zhang. 2019. "Machine learning of weld joint penetration from weld pool surface using support vector regression." *Journal of Manufacturing Processes* 41: 23-28.

Lias, SG, JE Bartmess, JF Liebman, JL Holmes, RD Levin, and WG Mallard. 2018. "Ion Energetics Data in NIST Chemistry WebBook, NIST Standard Reference Database Number 69." *National Institute of Standards and Technology, Gaithersburg MD* 20899.

Lieber, Daniel, Marco Stolpe, Benedikt Konrad, Jochen Deuse, and Katharina Morik. 2013. "Quality prediction in interlinked manufacturing processes based on supervised & unsupervised machine learning." *Procedia Cirp* 7: 193-198.

Lowke, John J, Richard Morrow, Jawad Haidar, and Anthony B Murphy. 1997. "Prediction of gas tungsten arc welding properties in mixtures of argon and hydrogen." *IEEE Transactions on plasma science* 25 (5): 925-930.

Lucas, W. 1992. "Shielding Gases for Arc Welding. I." *Welding and Metal Fabrication(UK)* 60 (5): 218.

Maxwell, Aaron E, Timothy A Warner, and Fang Fang. 2018. "Implementation of machine-learning classification in remote sensing: An applied review." *International Journal of Remote Sensing* 39 (9): 2784-2817.

Murphy, A Bo, M Tanaka, K Yamamoto, S Tashiro, To Sato, and JJ Lowke. 2009. "Modelling of thermal plasmas for arc welding: the role of the shielding gas properties and of metal vapour." *Journal of Physics D: Applied Physics* 42 (19): 194006.

Murphy, AB, M Tanaka, S Tashiro, T Sato, and JJ Lowke. 2009. "A computational investigation of the effectiveness of different shielding gas mixtures for arc welding." *Journal of Physics D: Applied Physics* 42 (11): 115205.

Najmon, Joel C, Sajjad Raeisi, and Andres Tovar. 2019. "Review of additive manufacturing technologies and applications in the aerospace industry." In *Additive manufacturing for the aerospace industry*, 7-31. Elsevier.

Nie, Zhenguo, Gang Wang, James D McGuffin-Cawley, Badri Narayanan, Shenjia Zhang, David Schwam, Michael Kottman, and Yiming Kevin Rong. 2016. "Experimental study and modeling of H13 steel deposition using laser hot-wire additive manufacturing." *Journal of Materials Processing Technology* 235: 171-186.

Okuyucu, Hasan, Adem Kurt, and Erol Arcaklioglu. 2007. "Artificial neural network application to the friction stir welding of aluminum plates." *Materials & design* 28 (1): 78-84.

Onsoien, M, R Peters, DL Olson, and S Liu. 1995. "Effect of Hydrogen in an Argon GTAW Shielding Gas: Characteristics and Bead Morphology." *Welding Journal* 74 (1): 10s-15s.

Oommen, Thomas, Debasmita Misra, Navin KC Twarakavi, Anupma Prakash, Bhaskar Sahoo, and Sukumar Bandopadhyay. 2008. "An objective analysis of support vector machine based classification for remote sensing." *Mathematical geosciences* 40 (4): 409-424.

Parvez, Shahid, Muhammad Abid, DH Nash, H Fawad, and Alexander Galloway. 2013. "Effect of torch angle on arc properties and weld pool shape in stationary GTAW." *Journal of Engineering Mechanics* 139 (9): 1268-1277.

Paskual, Amagoia, Pedro Álvarez, and Alfredo Suárez. 2018. "Study on arc welding processes for high deposition rate additive manufacturing." *Procedia Cirp* 68: 358-362.

Ranjan, Ravi, Aaquib Reza Khan, Chirag Parikh, Rahul Jain, Raju Prasad Mahto, Srikanta Pal, Surjya K Pal, and Debashish Chakravarty. 2016. "Classification and identification of surface defects in friction stir welding: An image processing approach." *Journal of Manufacturing Processes* 22: 237-253.

Renardy, Michael, Yuriko Renardy, and Jie Li. 2001. "Numerical simulation of moving contact line problems using a volume-of-fluid method." *Journal of Computational Physics* 171 (1): 243-263.

Ribic, B, R Rai, and Tarasankar DebRoy. 2008. "Numerical simulation of heat transfer and fluid flow in GTA/Laser hybrid welding." *Science and Technology of Welding and Joining* 13 (8): 683-693.

Shalev-Shwartz, Shai, and Shai Ben-David. 2014. *Understanding machine learning: From theory to algorithms*. Cambridge university press.

Silwal, Bishal, and Michalel Santangelo. 2018. "Effect of vibration and hot-wire gas tungsten arc (GTA) on the geometric shape." *Journal of Materials Processing Technology* 251: 138-145.

Singh, Akhilesh Kumar, Vidyut Dey, and Ram Naresh Rai. 2017. "Techniques to improveweld penetration in TIG welding (A review)." *Materials Today: Proceedings* 4 (2): 1252-1259.

Singh, Amanpreet, Narina Thakur, and Aakanksha Sharma. 2016. "A review of supervised machine learning algorithms." 2016 3rd International Conference on Computing for Sustainable Global Development (INDIACom).

Smola, Alex J, and Bernhard Schölkopf. 2004. "A tutorial on support vector regression." *Statistics and computing* 14 (3): 199-222.

Spaniol, E, T Ungethüm, M Trautmann, K Andrusch, M Hertel, and U Füssel. 2020. "Development of a novel TIG hot-wire process for wire and arc additive manufacturing." *Welding in the World*: 1-12.

Sumesh, A, K Rameshkumar, K Mohandas, and R Shyam Babu. 2015. "Use of machine learning algorithms for weld quality monitoring using acoustic signature." *Procedia Computer Science* 50: 316-322.

Tanaka, M, S Tashiro, To Satoh, AB Murphy, and JJ Lowke. 2008. "Influence of shielding gas composition on arc properties in TIG welding." *Science and technology of welding and joining* 13 (3): 225-231.

Teixeira, Paulo Roberto de Freitas, Douglas Bezerra de Araújo, and Luiz Antonio Bragança da Cunda. 2014. "Study of the gaussian distribution heat source model applied to numerical thermal simulations of TIG welding processes."

Thrysin, Erik, Gideon Gerhardsson, and Sven Forssman. 1952. "Fumes and gases in arc welding." *Arch. Indust. Hyg. & Occupational Med.* 6 (5): 381-403.

Tseng, KH, and CP Chou. 2002. "Effect of nitrogen addition to shielding gas on residual stress of stainless steel weldments." *Science and technology of welding and joining* 7 (1): 57-62.

Tseng, Kuang Hung. 2013. "Development and application of oxide-based flux powder for tungsten inert gas welding of austenitic stainless steels." *Powder technology* 233: 72-79.

Tseng, Kuang Hung, and Chih Yu Hsu. 2011. "Performance of activated TIG process in austenitic stainless steel welds." *Journal of Materials Processing Technology* 211 (3): 503-512.

Verma, Shubham, Meenu Gupta, and Joy Prakash Misra. 2018. "Performance evaluation of friction stir welding using machine learning approaches." *MethodsX* 5: 1048-1058.

Vidyarthy, RS, and DK Dwivedi. 2019. "Effect of shielding gas composition and activating flux on the weld bead morphology of the P91 ferritic/martensitic steel." *Materials Research Express* 6 (8): 0865f7.

Wang, Yan, Yi Sun, Peng Lv, and Hao Wang. 2008. "Detection of line weld defects based on multiple thresholds and support vector machine." *Ndt & E International* 41 (7): 517-524.

Wu, Bintao, Zengxi Pan, Donghong Ding, Dominic Cuiuri, Huijun Li, Jing Xu, and John Norrish. 2018. "A review of the wire arc additive manufacturing of metals: properties, defects and quality improvement." *Journal of Manufacturing Processes* 35: 127-139.

Wu, CS, QX Hu, and JQ Gao. 2009. "An adaptive heat source model for finite-element analysis of keyhole plasma arc welding." *Computational Materials Science* 46 (1): 167-172.

Xu, Xiangfang, Jialuo Ding, Supriyo Ganguly, Chenglei Diao, and Stewart Williams. 2018. "Oxide accumulation effects on wire+ arc layer-by-layer additive manufacture process." *Journal of Materials Processing Technology* 252: 739-750.

Zhou, Jun, and Hai Lung Tsai. 2007. "Effects of electromagnetic force on melt flow and porosity prevention in pulsed laser keyhole welding." *International Journal of Heat and Mass Transfer* 50 (11-12): 2217-2235.

APPENDIX A

DATA COLLECTED

Flowrate of 8 lpm.

N$_2$ %	Ar %	width (mm)	depth (mm)
0.00	100.00	4.79	2.02
0.09	99.91	5.3	2.36
0.11	99.89	4.9	2.24
0.11	99.89	4.82	2.41
0.31	99.69	4.78	2.4
0.38	99.62	5.08	2.41
0.63	99.37	4.82	2.44
0.95	99.05	5.06	2.76
1.10	98.90	5.12	2.52
1.27	98.73	5.2	2.8
1.39	98.61	5.13	2.81
1.59	98.41	5.24	2.82
1.91	98.09	5.32	2.81
1.91	98.09	5.2	2.84
2.24	97.76	5.56	2.88
2.56	97.44	5.52	2.91
2.70	97.30	5.37	2.57
2.89	97.11	5.68	2.72
3.23	96.77	5.5	2.85
3.36	96.64	5.56	2.71
3.56	96.44	5.66	2.76
3.90	96.10	5.61	2.9
3.90	96.10	5.78	2.97
4.23	95.77	5.86	2.98
4.58	95.42	6.08	3.06
4.79	95.21	5.63	3
4.92	95.08	5.88	3.02
5.18	94.82	5.83	2.91
5.26	94.74	6.01	2.71
5.54	94.46	5.95	2.91
5.61	94.39	5.96	3.12
5.96	94.04	6.06	2.95
6.31	93.69	6.28	3.36
6.67	93.33	6.4	3.04
6.67	93.33	6.21	3.34

Flowrate of 10 lpm.

N$_2$ %	Ar %	width (mm)	depth (mm)
0.00	100.00	5.13	2.53
0.50	99.50	5.18	2.55
1.01	98.99	5.22	2.61
1.52	98.48	5.27	2.6
2.04	97.96	5.39	2.56
2.56	97.44	5.34	2.67
3.09	96.91	5.47	2.5
3.63	96.37	5.4	2.62
4.17	95.83	5.46	2.61
4.71	95.29	5.81	2.82
5.26	94.74	5.83	2.86

Flowrate of 13 lpm.

N$_2$ %	Ar %	width (mm)	depth (mm)
0.00	100.00	5.3	2.51
0.39	99.61	5.56	2.53
0.78	99.22	5.55	2.5
1.17	98.83	5.5	2.58
1.56	98.44	5.66	2.59
1.96	98.04	5.65	2.78
2.36	97.64	5.75	2.63
2.77	97.23	5.77	2.8
3.17	96.83	5.7	2.74
3.59	96.41	5.86	3.03
4.00	96.00	5.9	3.08